Augmentation of heat transfer in a microtube and a wavy microchannel using hybrid nanofluid: A numerical investigation

Shikhar Kumar Singh[1], Suvanjan Bhattacharyya[2], Akshoy Ranjan Paul[1,*], Mohsen Sharifpur[3,4,*], Josua P. Meyer[3]

[1] Department of Applied Mechanics, Motilal Nehru National Institute of Technology Allahabad, Prayagraj, India

[2] Department of Mechanical Engineering, Birla Institute of Technology and Science, Pilani, Pilani Campus, Vidhya Vihar, Pilani, RJ, India

[3] Clean Energy Research Group, Department of Mechanical and Aeronautical Engineering, University of Pretoria, Pretoria, South Africa

[4] Institute of Research and Development, Duy Tan University, Da Nang, Vietnam

*Correspondence
Akshoy Ranjan Paul, Department of Applied Mechanics, Motilal Nehru National Institute of Technology Allahabad, Prayagraj, Uttar Pradesh, India. Email: arpaul@mnnit.ac.in

Mohsen Sharifpur, Clean Energy Research Group, Department of Mechanical and Aeronautical Engineering, University of Pretoria, Lynnwood Road, Pretoria, South Africa.
Email: mohsen.sharifpur@up.ac.za; mohsensharifpur@duytan.edu.vn

ABSTRACT

The paper discusses the numerical investigation involving forced convective heat transfer (HT) in the laminar flow regime is carried out for nanofluid (NF) and hybrid NF (HNF) in a microtube and wavy microchannel. Water-based Al_2O_3 NF and water-based Al_2O_3-Ag HNF is studied for this purpose. Reynolds number (Re), temperature, volume fraction, and nanoparticle (NP) size are varied for the analysis at a constant HT rate. Numerical results characterizing the performances of NF and HNF are presented in terms of the local HT coefficient. It is found that with the increase in Reynolds number, volume fraction, and temperature, local HT coefficient is increased. For Reynolds number of 50 and φ = 3%, a maximum of 11.03% increase in HT coefficient is obtained for microtube, while for the same case, a maximum of 10.16% is found for wavy microchannel. Comparison of NF and HNF reveals superior HT property of the later. However, microtube exhibits better HT coefficient than the wavy channel at constant heat flux, length, and area.

KEYWORDS : heat transfer, hybrid nanofluid, microtube, nanofluid, wavy microchannel

1 INTRODUCTION

One of the utmost achievements of technology in the 20th century is to put a relentless effect to move a thing toward miniaturization. Due to technological evolution and community move, either in the field of manufacturing, microelectronic, transportation, space research, thermal

power plant, and so forth, need to develop smaller systems which cause intense heat generation. This requires an efficient coolant which can dissipate heat at a faster rate. Traditional coolants like ethylene glycol, water, transformer oil, and propylene glycol have low thermal conductivity (TC) value, making them inappropriate candidates in miniaturizing world. So, a novel fluid is required, which contains a high value of TC and for that one has to incorporate NPs in the base fluid, which is having much higher value of conductivity than base fluid. This eventually gave the birth of a highly efficient cooling fluid, which is termed as nanofluid (NF). NFs are the mixture of solid and liquid with particle size less than a hundred nanometers, and the value of TC of NFs is greater than water, which will be the base fluid. This NF dissipates more thermal energy due to the high value of TC, and subsequently, it enhanced the thermohydraulic performance of the system. The cooling aspect in microchannel was first introduced by Tuckerman and Pease.[1] NF term was first coined by Choi and Eastman.[2] After that, NFs get popularity due to better cooling capability.

To enhance the TC, dispersion of a solid particle in the liquid is not a new concept. Theoretically, it was introduced by Maxwell.[3] Despite numerous studies from the last century on TC using conventional solid/liquid suspension containing millimeter- or micrometer-sized particle, rapid settling of these suspensions becomes a major hurdle to develop suspension for particle application. The two salient features of NFs—higher TC and well-suspended particles—make NF a strong candidate for next-generation coolant for the thermal management system. At the early stage, the model proposed by the investigators for the TC of NFs considered NPs as stagnant. Classical models consider very few parameters for the calculation of TC, but as the development goes on more and more, a realistic model comes into account which considers more physical parameters, but still, there was no such model available in the literature which can predict all the insight of NFs. The first model was introduced by Maxwell,[3] and later on, a number of models[4-15] were introduced to calculate the TC of NFs. Keblinski et al[16] recommended four possible reasons for the higher TC of NFs. The reasons are like Brownian motion done by ultrafine NFs, liquid layer formation around the nanoparticle which has a high value of TC than water (base fluid), nature of heat transfer is ballistic rather than diffusive augmenting the conduction HT due to the smaller size of nanoparticle, and conduction heat transfer takes place at a faster rate rather than convective HT due to nanoparticle clustering.

Modeling the TC of hybrid NF (HNF) is a very complex phenomenon. Very few models for TC of HNFs are present in literature, and all the models pertain to a particular type of HNF under certain specific conditions. The temperature plays a major role in TC at a higher volume fraction for HNF. Esfe et al[17] used an artificial neural network (ANN) to calculate the TC of Cu/TiO_2-water/EG HNF. The model included the effect of temperature and particle volume fraction. Toghraie et al[18] considered $ZnO\text{-}TiO_2$/EG HNF to study the influence of particle temperature and volume fraction on its TC. Parsian and Akbari[19] proposed a model to estimate the effective TC of the HNF. The model forecasts the TC of HNF with great accuracy, but it requires a greater insight of nanoparticle and base fluid.

After TC, viscosity is the second most significant parameter in modeling NFs. To mimic the behavior of NF and HNF with greater accuracy, viscosity plays a vital role. Einstein[20] first presented a model for viscosity. The model has constraint that it is only applicable for a spherical-shaped particle in the range of particle concentration of ($\varphi < 0.02$ *vol*). Einstein's

viscosity formula is considered as the fundamental equation for viscosity, and many researchers contribute to this equation. Brinkman[21] and Batchelor[22] extended the applicability of Einstein's viscosity relation to a moderate particle volume concentration up to 4%. Several researchers[23-25] eventually come up with robust model for the estimation of viscosity of NFs. Corcione[14] proposed a correlation for estimating dynamic viscosity for NFs by using large experimental data and has been quite useful in modeling NF viscosity.

In literature, forced convection HT behavior of NFs was modeled by either two-phase or single-phase approach. Two-phase methods either provide better result and understanding of nanoparticles and fluid phase, but the problem with two-phase approach is that it is computationally more intensive and does not require when the focus is only on heat transfer analysis. In the present study, a single-phase approach is considered because it is simple to implement, and nanoparticle behaves like a single-phase mixture. In single-phase, the symmetry between the fluid phase and the NF phase is considered. Though, in the present study, thermal dispersion effect is considered due to the chaotic nature of NFs in the flow.

Metal oxide nanoparticles, like Al_2O_3 nanoparticle, exhibit excellent stability and chemical inertness, but it has poorer TC while silver (Ag)—a metallic nanoparticle shows higher TC, but it is unstable in chemical point of view and reactive. By hybridizing these NPs, one can get a fluid which shows superior rheological behavior and thermophysical properties together with the advanced HT characteristics. A similar type of hybridization gives the birth of extremely efficient coolant named as HNFs. HNF is not a new concept but the extension of the previous one. They are homogeneous in nature with novel chemical and physical properties. The main idea of HNF is to attain a higher HT rate compared to single NFs. Turcu et al[26] introduced the concept of HNF by synthesizing the polypyrrole-carbon nanotube with Fe_2O_3 nanoparticles. HNF is a new concept, and very limited literature is therefore available. Literature suggests that very few correlations are developed for HNFs, and the correlations which were developed are for specific HNFs under the certain limit of temperature and nanoparticle concentration.

A few researchers[27, 28] worked on HT characteristics of NFs in microchannel, while Leala and Nisulescu[29] studied the same in a microtube (MT). Later, Nimmagadda and Venkatasubbaiah[30] and Selvakumar and Suresh[31] investigated the transport behavior of HNF in a microchannel while Yang et al[32] and Sakanov et al[33] focussed on HNF behavior in a wavy microchannel (WC). Bhattacharyya et al[34-38] studied computationally and experimentally the influence of vortex generators in forced convection to enhance heat transfer.

These studies generally focused on TC rather than the HT coefficient. HNFs are very new in the field of research, and very limited research work is available in the literature. There is hardly any research work available which compared the effect of different parameters on NFs and HNFs in a MT and WC.

Chamkha and coworkers[39-53] have investigated the forced and mixed convection numerically through noncircular and circular channels by using different NFs (acting alone with base fluid) and HNFs. Sharifpur and coworkers[54-59] also investigated numerically and experimentally the thermo-convection performance of HNFs and single-particle NFs. Similarly, Ahmadi and coworkers[60-68] also investigated numerically and experimentally the thermal performance of

and mono-particles NFs and HNFs in micro, mini, and conventional circular and noncircular channels. In recent years, a surge of literature on heat transfer using NFs have been noticed. In the year 2018, researchers like Dogonchi et al,[69] Esfe et al,[70] Ghahremani,[71] Izadi et al,[72] and Mehryan et al[73] studied free convection of various NFs (Cu-water, Al_2O_3-water, and ferro-fluids) under magnetic fluids. The trend continued in the year 2019 with the researchers like Alsabery et al,[74] Dogonchi et al,[75] Hoseinzade et al,[76] Kumar et al,[77] Shashikumar et al,[78] Sobamowo,[79] Tayebi and Chamkha,[80] Ghalambaz et al,[81] and Ghalambaz et al[82] who investigated natural and mixed convection on NF-filled porous cavities and fins under the influence of magnetic field and/or thermal radiation. Similar research initiatives continued in the following year as well with researchers like Alsabery et al,[83] Dogonchi et al,[84] Hajjar et al,[85] and Hashemi-Tilehnoee et al[86] who explored natural and mixed convection effects in NF filled lid-sriven cavities and wavy geometry under the influence of magnetohydrodynamic field. However, only a handful of researchers like Chamkha et al,[87] Mehryan et al,[88] and Ghalambaz et al[87] reported on HNFs during this period, which motivated the present authors to conduct the numerical analysis of HNFs in different channels and enclosures.

The detailed literature review reveals that there is a need of further study of the behavior of HNF (the main reason of employing Al_2O_3-Ag nanoparticles is by following experimental work of Aparna et al[89] and Jastrzebska et al[90]) in vaious types of MTs and microchannels. Since there was a dearth of literature in a WC, hence a WC is considered in the current study. The objective of the current numerical investigation is, therefore, to analyze the flow characteristics of NF and HNF. For this, the local HT coefficient is considered as a performance parameter. The geometrical effect of the flow path is also analyzed using MT and WC. The effects of Re, volume fraction, temperature, and nanoparticle size are studied in detail.

2 COMPUTATIONAL METHODOLOGY

2.1 Geometry

In the present study, an MT is considered as shown in Figure 1. Since this geometry is symmetrical, the two-dimensional axisymmetric domain is considered here. For generation of the computational domain, Ansys-Design modeler was used. A rectangular computational domain is generated in the Cartesian coordinate system with the origin located at the inlet of the MT. A computational domain of the problem is given in Figure 2.

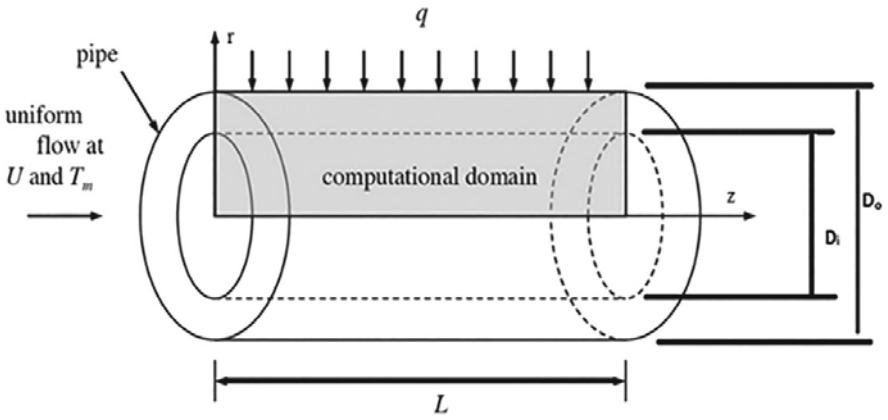

FIGURE 1. The schematic diagram of the microtube

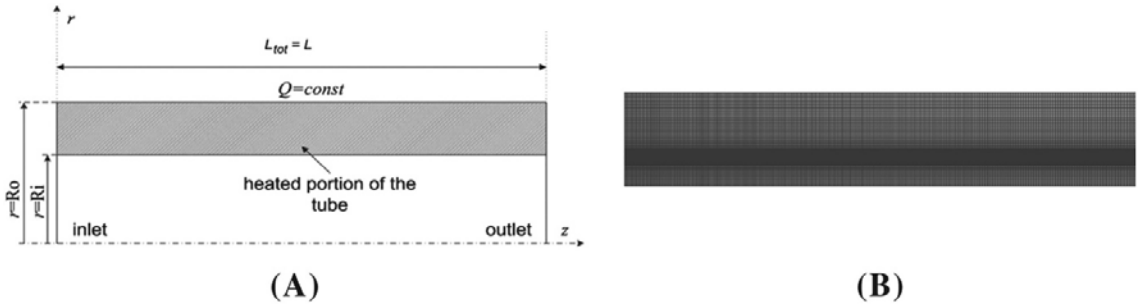

FIGURE 2. (A) The schematic diagram of computational domain for microtube, and (B) mesh of microtube

A two-dimensional wavy channel is also considered for the study, as shown in Figure 3. The geometry of the wavy channel is chosen such that its fundamental dimensions are matched with the dimensions of the MT. The height of the fluid domain is 0.1 mm, total thickness of the wavy channel is 0.2 mm, and length of the wavy channel is 100 mm. All these parameters are the same as in the case of the MT. Tables 1 and 2 furnish all the dimensions of the MT and wavy channel used in the study.

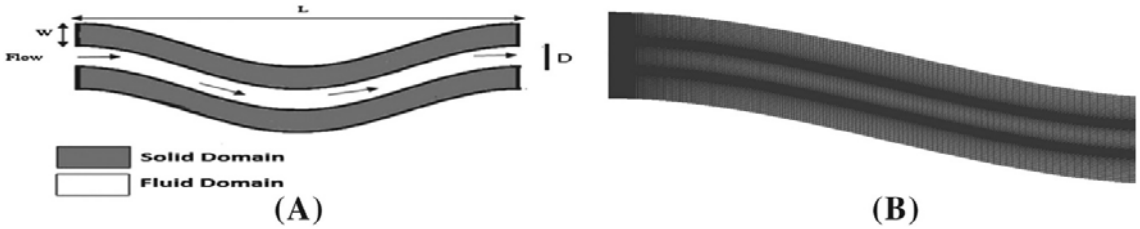

FIGURE 3. (A) Schematic diagram of a wavy microchannel, and (B) mesh of wavy microchannel

TABLE 1. Dimensions of microchannel

Parameter	Value
Length of channel (L)	100 mm
Inner diameter	0.1 mm
Outer diameter	0.3 mm
Thickness	0.2 mm

TABLE 2. Dimensions of wavy channel

Parameter	Value
Length of channel (L)	100 mm
Wavelength (λ)	4 mm
Hydraulic diameter (Dh)	0.2 mm
Thickness (w)	0.1 mm

2.2 Grid generation

The computational domain of the problem is discretized into a number of grids/mesh as shown in Figures 2B and 3B. To discretize the domain, mesh modeler available in ANSYS Fluent 16.0 is used. The fluid domain of the MT is divided into 70 and 2,500 elements in radial and axial directions, respectively, while the solid domain contains 50 and 2,500 elements in radial and axial directions, respectively, and thus constituted 302,621 elements in the whole geometry. The fluid domain of the wavy channel is divided into 3,900 elements in axial directions and 70 elements along with the thickness, while the solid domain contains 3,900 elements in the axial direction and 60 elements along with the thickness and thus it constituted 358,800 elements in the whole geometry.

To verify the sensitivity of the studied grid, three mesh sizes are compared. Heat transfer coefficient is considered as the governing parameter to verify the sensitivity of the studied grid. For MT geometry, three grids, namely coarse (60 × 2000), medium (70 × 2,500), and fine (80 × 3,000), are considered for the fluid domain. For medium and fine grids, the successive difference in the heat transfer coefficient is only 0.059%. Hence, the medium grid (70 × 2,500) is selected for the MT geometry. For the wavy channel, three grids of 328,350 (coarse), 358,800, (medium) and 366,300 (fine) elements are generated. For medium and fine grid sizes, the successive difference in the heat transfer coefficient of 0.11% is accounted. Hence, the medium quality grid having 358,800 elements is selected for further computational investigation.

2.3 Mathematical formulation

The following set of partial differential equations in the cylindrical coordinate system is used to describe the phenomenon, considering the effective thermophysical properties of the fluids[91]:

Continuity equation,

$$\frac{\partial(\rho_{eff}.u)}{\partial z}+\frac{1}{r}\frac{\partial(r.\rho_{eff}.v)}{\partial r}=0.$$

Momentum equation,

$$\frac{\partial(\rho_{eff}vu)}{\partial r}+\frac{\partial(\rho_{eff}uu)}{\partial z}=-\frac{dp}{dz}+\frac{1}{r}\frac{\partial}{\partial r}\left(\mu_{eff}r\frac{\partial u}{\partial r}\right).$$

Energy equation,

$$\frac{\partial(\rho_{eff}c_{peff}vT)}{\partial r}+\frac{\partial(\rho_{eff}c_{peff}uT)}{\partial z}=\left[\frac{1}{r}\frac{\partial}{\partial r}\left(k_{eff}.r\frac{\partial T}{\partial r}\right)+\frac{\partial}{\partial z}\left(k_{eff}\frac{\partial T}{\partial z}\right)\right]+\mu_{eff}.S_v$$

For estimating the effective TC of NF, a theoretical correlation given by Chon et al[9, 92] is used in the present study, and it is described as follows:

$$\frac{keff}{kbf}=1+64.7(\phi)^{0.7640}\left(\frac{dbf}{dnp}\right)^{0.3690}\left(\frac{kbf}{knf}\right)^{0.7476}Pr_T^{0.9955}Re^{1.231}.$$

For estimating effective dynamic viscosity of NF, the model of Corcione[14] is used, which involves temperature-dependent effective dynamic viscosity and is given as follows:

$$\frac{\mu_{eff}}{\mu_{bf}} = \frac{1}{\left(1 - 34.87\left(\frac{d_p}{d_{bf}}\right)^{-0.3}\phi^{1.03}\right)}.$$

For estimating the effective TC of HNF, the model of Aparna et al[89] is used, and the theoretical correlation is described as follows:

$$k_{eff} = A + (B \times \phi) + (C \times T) + (D \times \phi \times T).$$

For estimating effective viscosity of HNF, the model of Batchelor[22] is used, which is described as follows:

$$\mu_{eff} = \left(1 + 2.5\phi + 6.2\phi^2\right)\mu_{bf}.$$

Density and specific heat of NF are calculated as follows:

$$\rho_{eff} = (1 - \phi)\,\rho_{bf} + \phi\rho_{np},$$

$$C_{peff} = \frac{(1 - \phi).\,(\rho.\,C_p)_{bf} + (\rho.\,C_p)_{np}}{\rho_{eff}}.$$

Specific heat and density of HNF are calculated as follows:

$$\rho_{eff})_{hybrid} = \phi_{np1}\,\rho_{np1} + \phi_{np2}\,\rho_{np2} + (1 - \phi)\,\rho_{bf}$$

$$C_{p,eff})_{hybrid} = \frac{(1 - \phi)\,\rho_{bf}\,C_{p,bf} + \phi_{np1}\,\rho_{np1}\,C_{p,np1} + \phi_{np2}\,\rho_{np2}\,C_{p,np2}}{\rho_{eff}}$$

The values of thermophysical properties (like effective density and effective specific heat) are depicted in Tables 3 and 4 for NF and in Tables 5 and 6 for HNF based on data presented in previous studies.[29, 91]

TABLE 3. Effective density of Nanofluid

ϕ	Density of water (kg/m^3)	Density of Al_2O_3 (kg/m^3)	Effective density
0.01	998.2	3,975	1,027.968
0.02	998.2	3,975	1,057.736
0.03	998.2	3,975	1,087.504

TABLE 4. Effective specific capacity of nanofluid

ϕ	C_p of water (J/kg-K)	C_p of Al_2O_3 (J/kg-K)	Effective C_p
0.01	4,182	765	4,049.869
0.02	4,182	765	3,925.176
0.03	4,182	765	3,807.309

TABLE 5. Effective density of hybrid nanofluid

ϕ of Al_2O_3	ϕ of Ag	Density of Al2O3 (kg/m^3)	Density of Ag (kg/m^3)	Density of water (kg/m^3)	Effective density
0.005	0.005	3,975	10,500	998.2	1,060.593
0.01	0.01	3,975	10,500	998.2	1,122.986
0.015	0.015	3,975	10,500	998.2	1,185.379

TABLE 6. Effective specific capacity of hybrid nanofluid

ϕ of Al_2O_3	Density of Al_2O_3	C_p of Al_2O_3	ϕ of Ag	Density of Ag	C_p of Ag	C_p of water	Density of water	Effective density	Effective C_p
0.005	3,975	765	0.005	10,500	235	4,182	998.2	1,060.593	3,921.077
0.01	3,975	765	0.01	10,500	235	4,182	998.2	1,122.986	3,679.589
0.015	3,975	765	0.015	10,500	235	4,182	998.2	1,185.379	3,463.522

The stability of NPs are very important, and Aparna et al[89] have done the stability analysis, and it was experiential that the stability of Al_2O_3-Ag NF having a mix ratio of 30:70 or 70:30 is less than 2 h. However, it has been found that in 24 h, Al_2O_3-Ag NF is having a mix ratio of 50:50. Hence, Al_2O_3-Ag NF having a mix ratio of 50:50 is taken for the study.

2.4 Boundary conditions

Boundary conditions applied for MT and wavy channel are furnished in Table 7. Uniform temperature and velocity are imposed at the entry (inlet) of MT and wavy channel, as shown in Table 8. The outflow boundary condition is given at the MT and wavy channel outlet. Uniform heat flux is specified at the outer surface of the MT and wavy channel.

- **Inlet**: Uniform temperature and velocity field is given as follows

$$\mathbf{X = 0, 0 < r < R_o : u = U, T = T_{wall} = T_o.}$$

TABLE 7. Boundary condition for microtube and wavy channel

Boundary	Boundary conditions	
	For microtube	For wavy channel
Fluid inlet	Velocity inlet	Velocity inlet
Fluid outlet	Outflow	Outflow
Flux wall	Wall (constant heat flux)	Wall (constant heat flux)
Fluid domain	Fluid	Fluid
Solid domain	Solid	Solid
Interface wall	Wall (conjugate heat transfer)	Wall (conjugate heat transfer)
Axis	Axis	

TABLE 8. The values of the inlet velocity and temperature for microtube and wavy channel

- **Outlet**: The gradient of temperature and velocity normal to the exist plane is kept zero.

$$\mathrm{Z} = \mathrm{L}: \frac{\partial u}{\partial r} = 0 \frac{\partial T}{\partial r} = 0.$$

- **Outer solid wall**: Uniform heat flux is applied on the outer surface of the solid wall

$$\mathrm{r} = \mathrm{R_o}: q_o = k_s \frac{\partial T}{\partial z} - 0,$$

where q_0 is the uniform heat flux imposed on the outer surface of the wall.

- **Conjugate heat transfer**: The conjugate heat transfer implies that the continuity of temperature and heat flux at the solid-liquid interface is defined as

$$r = R_i: T_s | R_{i+} = T_f | R_{i-},$$

$$k_s \left(\frac{\partial T_s}{\partial r} \right)_{R_i+} = k_{eff} \left(\frac{\partial T_f}{\partial r} \right)_{R_i-}.$$

In the case of NF, a UDF is used to incorporate the TC and viscosity, whereas in the case of HNF, UDF is used to incorporate TC only. For pressure, a second-order discretization scheme is used. A higher-order QUICK scheme is used, while for energy, a second-order UPWIND scheme is used.[34-36, 38, 93-97] A semi-implicit method for the pressure-linked equations-consistent algorithm is used for pressure-velocity coupling. Finite volume method (FVM) is used to solve the partial differential equations and boundary condition together. Convergence criteria for continuity, velocity components, and temperature are kept at 10^{-6}.

2.5 Validation of the model

The results acquired from the current numerical investigation are compared with Lelea and Nisulescu.[29] Taking other test parameters constant at two different particle volume concentrations ϕ = 1% and 4%, a numerical simulation is carried out. The results of both validations are presented in Figure 4A,B. The maximum deviations obtained are 4.5% and 4.78% at ϕ = 1% and 4%, respectively, which is up to an acceptable level.

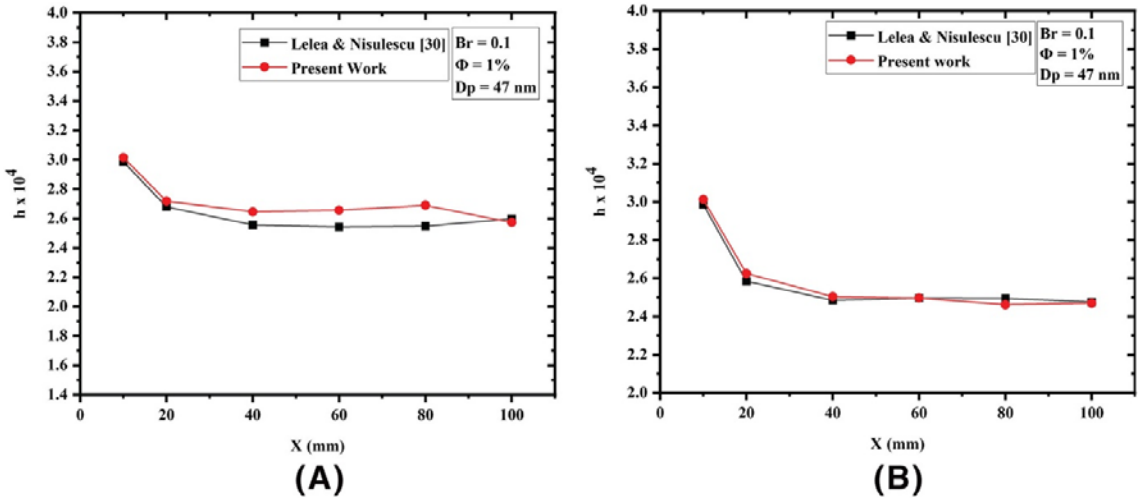

FIGURE 4. Validation: (A) at ϕ = 1% and (B) at ϕ = 3%

3 RESULTS AND DISCUSSION

The influences of various parameters, like Re, temperature, and particle volume fraction and NPs size, are studied and furnished in subsections.

3.1 Influence of Reynolds number

In this section, Reynolds number (Re) is varied at 50, 100, 250, 500, 750, and 1,000 for both the NF and HNF flowing through a nanotube and WC for different particle volume fractions.

Effect of Reynolds number on NF in MT at volume fractions 1% and 3% are shown in Figure 5A,B. One can see from the figures that for NF flowing through MT, with an increase in Re, HT coefficient (*h*) increases.

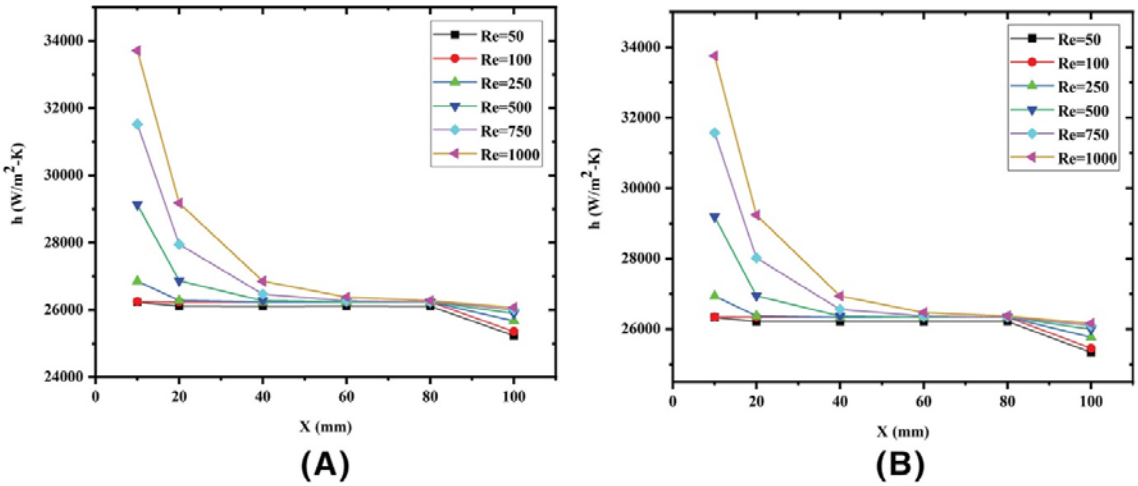

FIGURE 5. Effect of Reynolds number on nanofluid in microtube: (A) at ϕ = 1% and (B) at ϕ = 3%

Influence of Re on HNF in MT at volume fractions 1% and 3% are shown in Figure 6A,B. Similar results are depicted for HNF flowing in MT as well in Figure 6. The value of *h* becomes almost constant at a shorter distance. Some abnormality is, however, found in *h* at lower Reynold Numbers for both Figures 5 and 6. The value of *h* exhibits a rise in the axial direction, and these phenomena are more prominent at higher particle volume fraction.

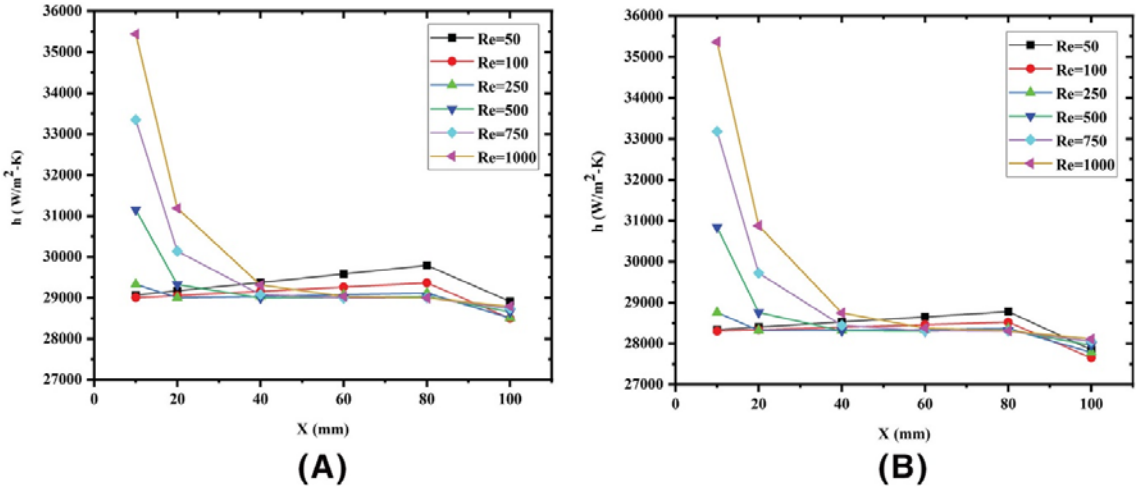

FIGURE 6. Effect of Reynolds number on hybrid nanofluid in microtube: (A) at ϕ = 1% and (B) at ϕ = 3%

Effect of Reynolds number on NF in the wavy channel at volume fractions 1% and 3% are shown in Figure 7A,B, and the effect of Reynolds number on HNF in wavy channel at volume fractions 1% and 3% are shown in Figure 8A,B. In case of NF flowing through the WC, *h* becomes constant and independent of Reynolds number at a much shorter distance in the axial direction as compared to MT (Figures 7 and 8). Heat transfer coefficient value for HNF increases as it moves in the axial direction, and the rise is more prominent for higher volume fraction in Figure 8.

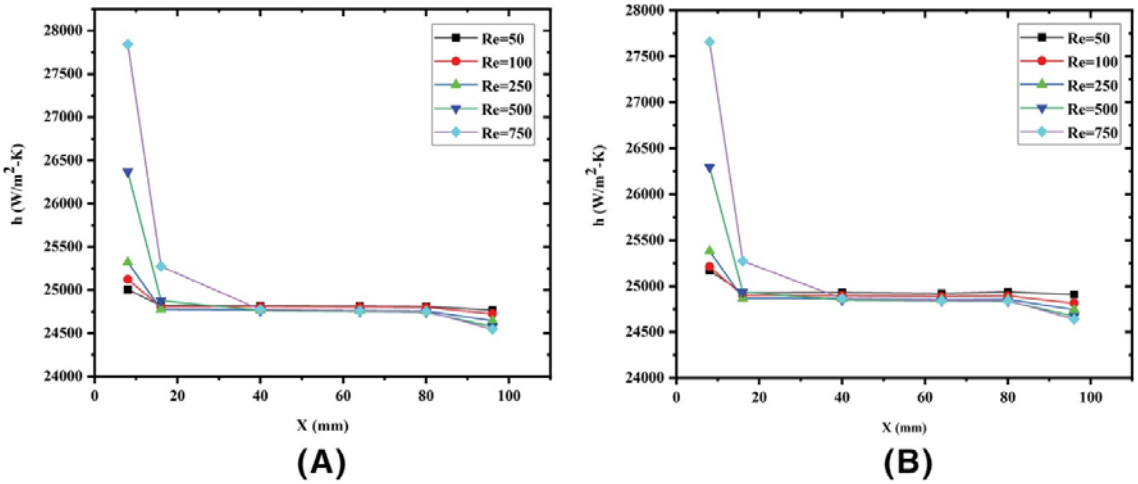

FIGURE 7. Effect of Reynolds number on nanofluid in wavy channel: (A) at ϕ = 1% and (B) at ϕ = 3%

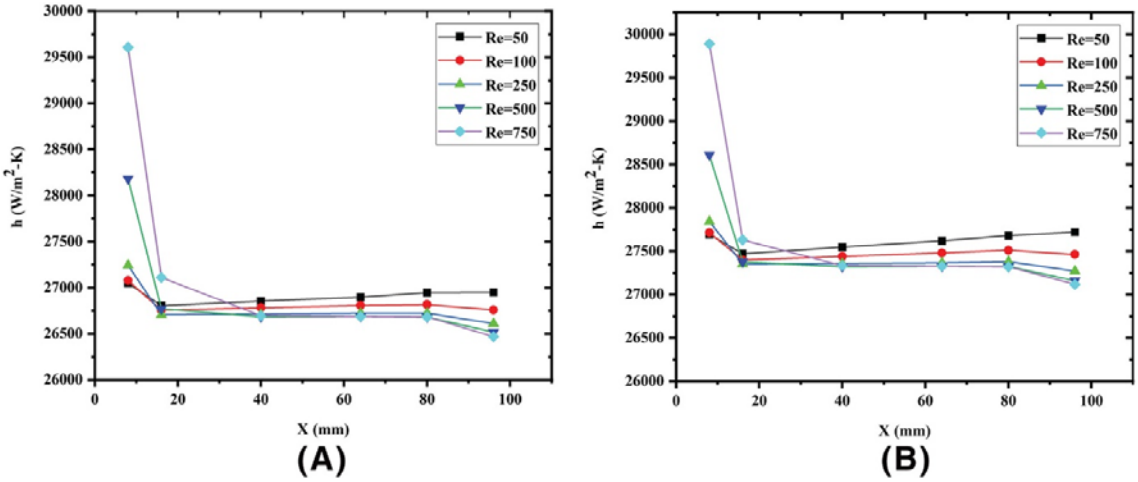

FIGURE 8. Effect of Reynolds number on hybrid nanofluid in a wavy channel: (A) at ϕ = 1% and (B) at ϕ = 3%

3.2 Influence of particle volume fraction

The present study is done with an assumption that NF is a single-phase fluid. With the increase in volume fraction, it moves toward multiphase fluids. This constraint makes the variation of volume fraction up to a certain limit. Though, in the literature we find that up to 4% of the variation in the result is in the tolerable limit. Considering this thing in mind, the variation of volume fraction is up to 4%. When NPs' concentration rises, the TC will be improved; however, on the other side, beyond the certain concentration of NPs, pressure drop rises, which is not noteworthy for thermal energy systems.[98]

Influence of volume fraction on NF in MT at different Reynolds number (Re 50 and 1,000) are shown in Figure 9A,B. With a rise in particle volume fraction (ϕ), *h* increased on NF in the MT. But, nature is not the same when varying with Reynolds number. At lower Reynolds number, with an increase inϕ, *h* increased significantly. HT coefficient becomes constant in the axial direction at lower Reynolds number, as shown in Figure 9A. At higher Reynolds number, the effect of volume fraction, however, becomes negligible and *h* becomes independent of volume fraction as shown in Figure 9B. A decrease in *h* is registered as one move in the axial direction.

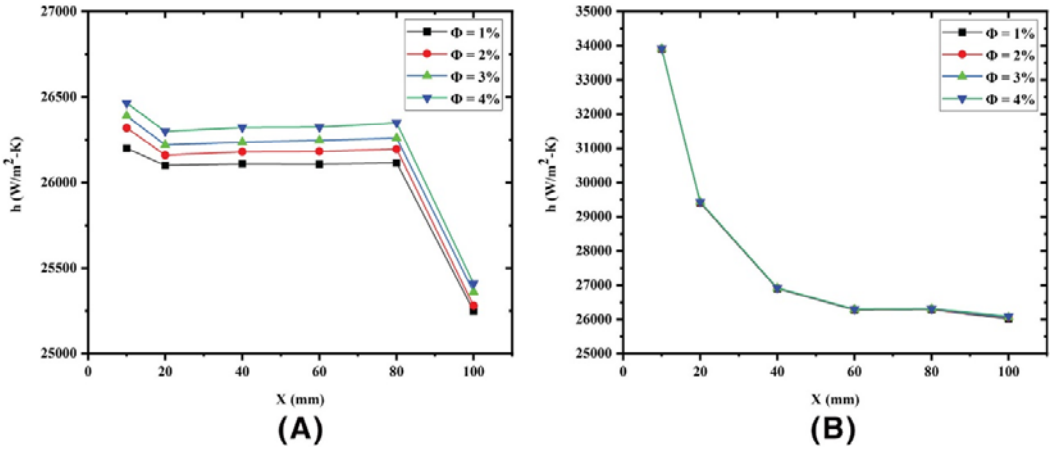

FIGURE 9. Effect of volume fraction (ϕ) on nanofluid in microtube: (A) at *Re* = 50 and (B) at *Re* = 1,000

Effect of volume fraction on HNF in MT at different Reynolds numbers (Re 50, 250, 500, and 1,000) are shown in Figure 10A-D. The same trend is found for HNF in MT, that is, with an increase in volume fraction, *h* is increased. At a lower Reynolds number, the influence of ϕ is more significant as compared to the higher Re as shown in Figure 10. Heat transfer coefficient *h* increases in the axial direction at lower Reynolds number, and a reverse trend is found for higher Reynolds number for HNF in a MT.

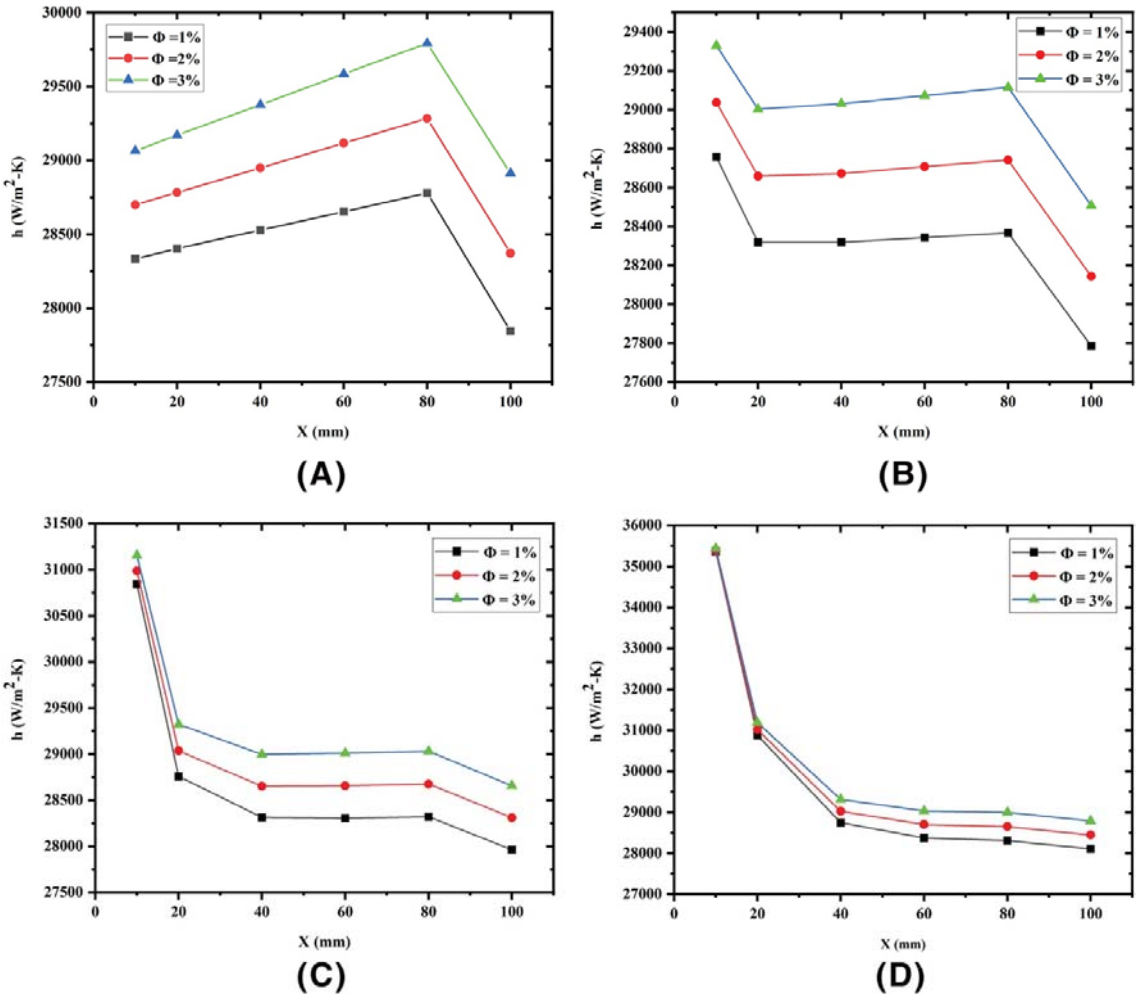

FIGURE 10. Effect of volume fraction (ϕ) on hybrid nanofluid in microtube: (A) at Re = 50, (B) at Re = 250, (C) at Re = 500, and (D) at Re = 1,000

Volume fraction variations are significant for the WC. Effect of volume fraction on NF in the WC at different Reynolds numbers (Re 50 and 1,000) are shown in Figure 11A,B. For NF flowing through the WC, with an increase in ϕ, *h* is increased. Influence of ϕ is more noteworthy at lower Reynolds number. Heat transfer coefficient *h* becomes almost constant in the axial direction at lower as well as for higher Re as presented in Figure 11A,B.

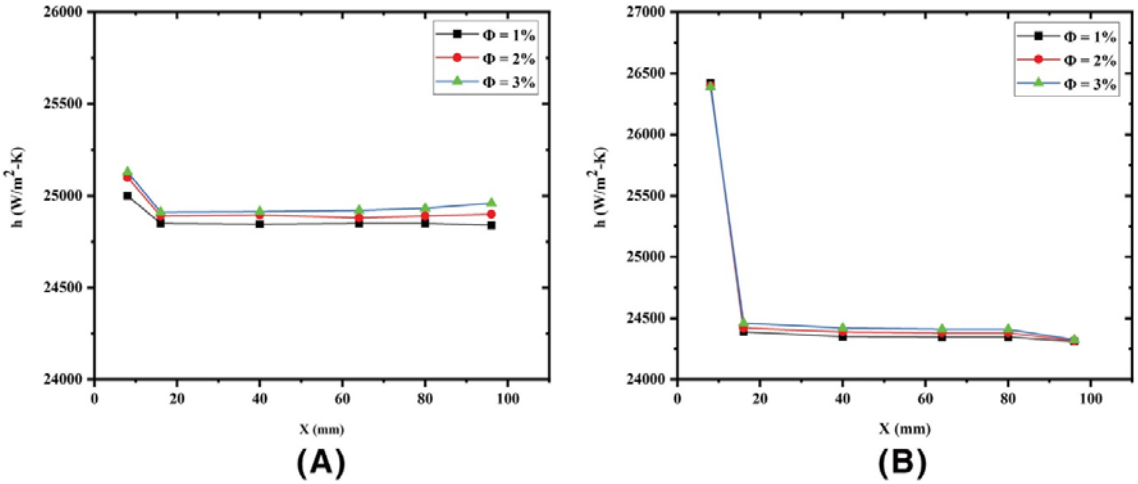

FIGURE 11. Effect of volume fraction (ϕ) on nanofluid in wavy microchannel: (A) at Re = 50 and (B) at Re = 1,000

Effect of volume fraction on HNF in the WC at different Reynolds numbers (Re 50, 250, 500, and 1,000) are presented in Figure 12A-D. With the increase in ϕ for the HNF flowing through a WC, h is increased. At lower Re, h increases along axial direction at lower Reynolds number, and it became almost constant at higher Re. The effect of ϕ is more significant at lower Re as compared to the higher Re as presented in Figure 12.

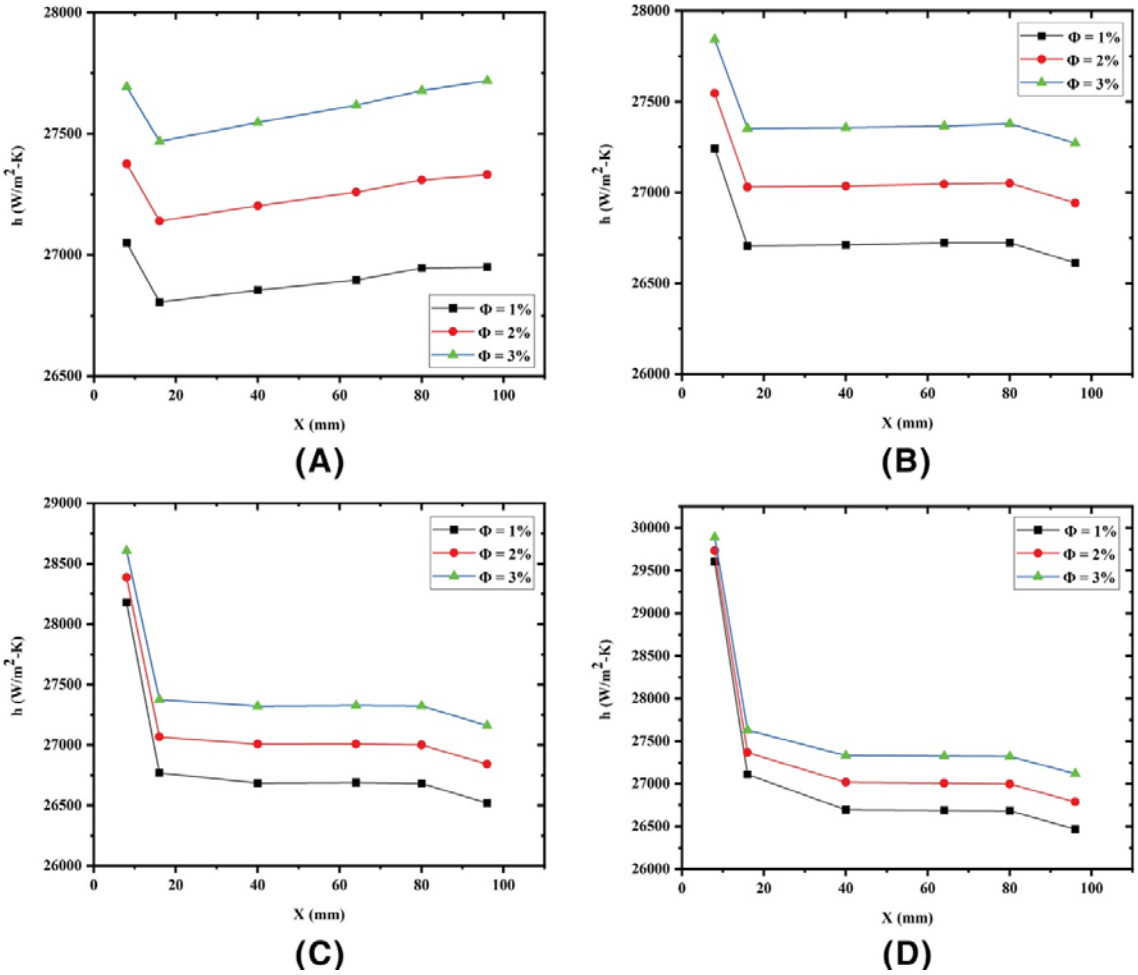

FIGURE 12. Effect of volume fraction (ϕ) on hybrid nanofluid in wavy microchannel: (A) at Re = 50, (B) at Re = 250, (C) Re = 500, and (D) Re = 1,000

3.3 Effect of temperature

To investigate the influence of inlet fluid temperature, it is varied in a range of 293 to 314 K, and the results are furnished in this section. The influences of temperature on NF at MT at different Reynolds numbers (Re 50 and 1,000) are shown in Figure 13A,B. For NF flowing through the MT, *h* increases marginally with increase in inlet fluid temperature as depicted in the figure.

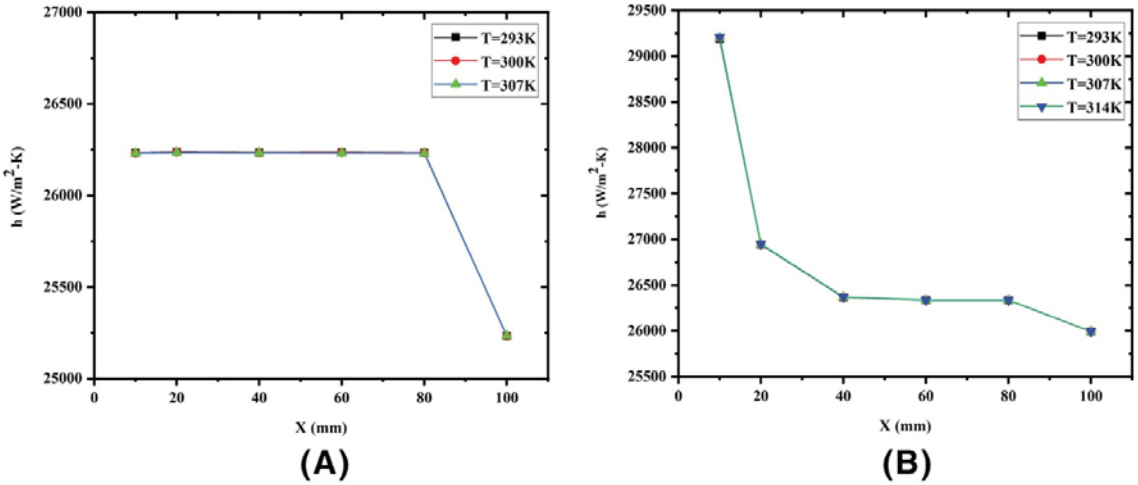

FIGURE 13. Effect of temperature on nanofluid at in microtube: (A) at Re = 50 and (B) at Re = 1,000

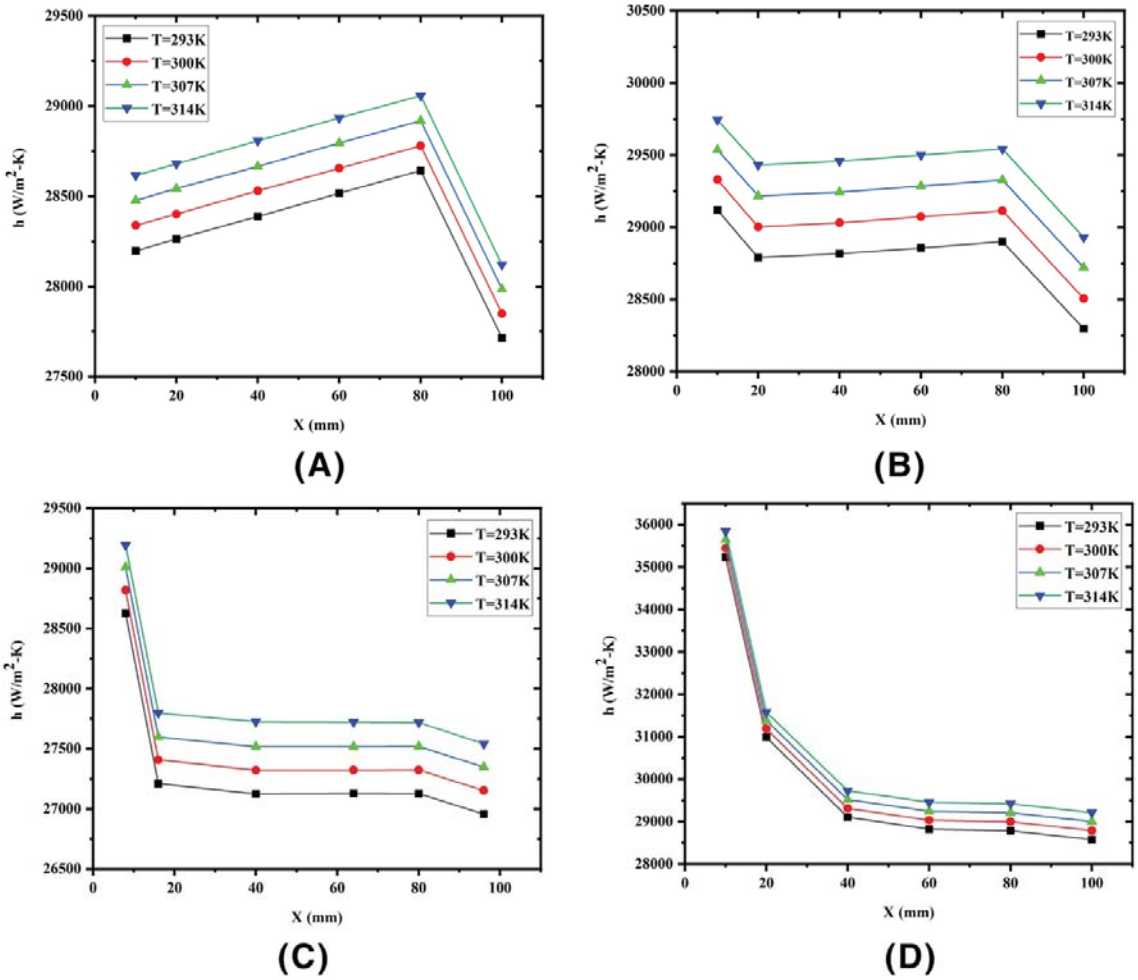

FIGURE 14. Effect of temperature on hybrid nanofluid at φ = 3% in microtube: (A) at Re = 50, (B) at Re = 250, (C) Re = 500, and (D) Re = 1,000

The influences of temperature on HNF at MT at different Reynolds numbers (Re 50, 250, 500, and 1,000) are presented in Figure 14A-D. A significant effect of temperature is found for HNF

flowing in the MT as it is seen from Figure 14 that with a rise in temperature, *h* is increased, especially at a low Reynolds number range.

The effects of temperature on NF at WC at different Reynolds numbers (Re 50 and 1,000) are shown in Figure 15A,B. No such effect of temperature is, however, found on NF in WC as depicted in the figures. The effects of temperature on HNF at in WC at different Reynolds numbers (Re 50, 250, 500, and 1,000) are presented in Figure 16A-D. A significant effect of temperature is found for HNF flowing in a WC. From the figures, one can easily see and notice that *h* increases with a rise in temperature.

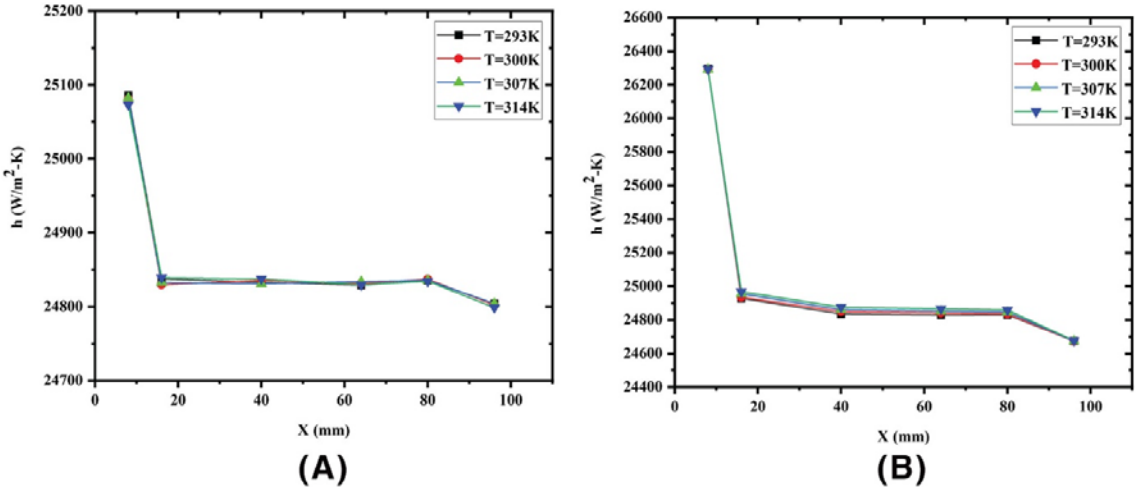

FIGURE 15. Effect of temperature on nanofluid at in a wavy microchannel: (A) Re = 50 and (B) Re = 1,000

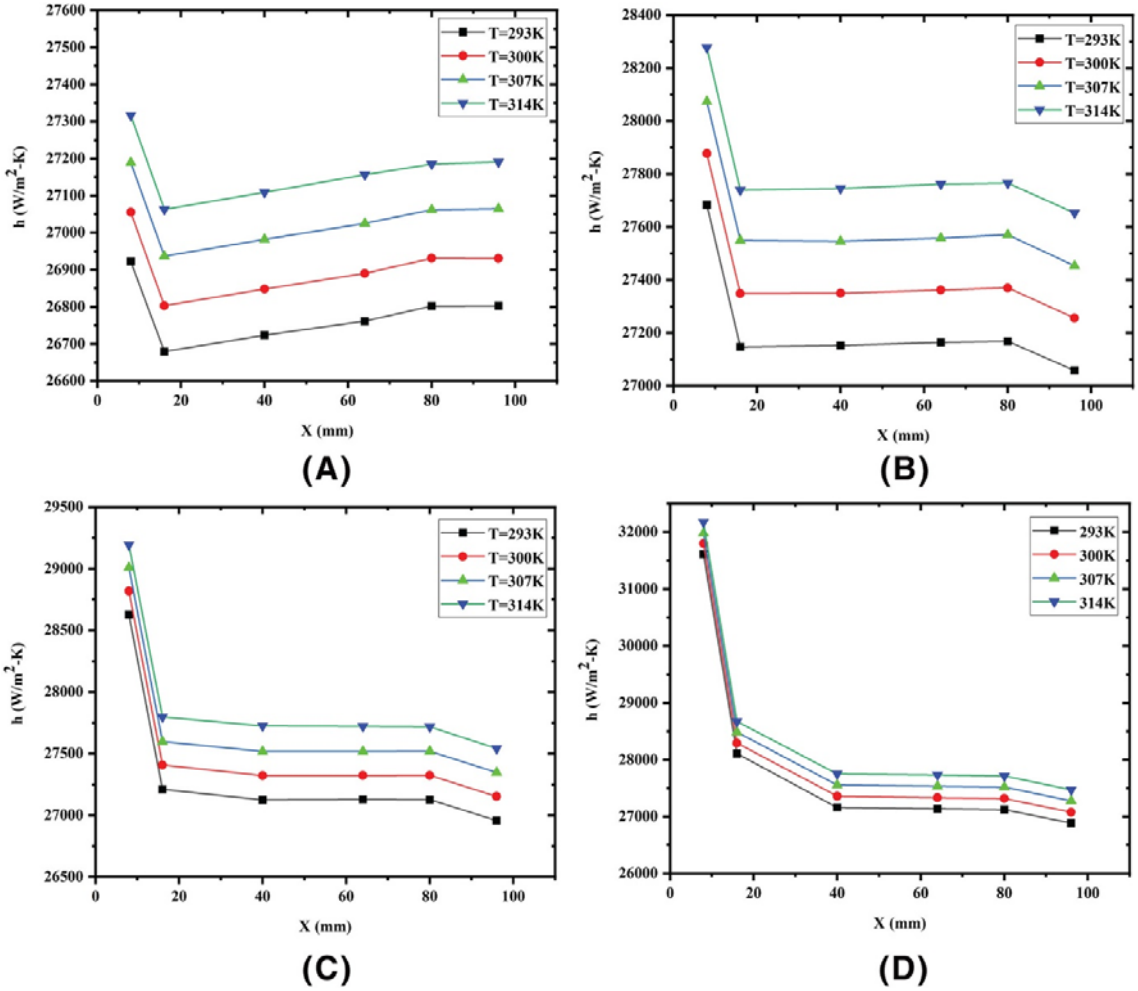

FIGURE 16. Effect of temperature on hybrid nanofluid at ϕ = 3% in a wavy microchannel: (A) Re = 50, (B) Re 250, (C) Re = 500, and (D) Re = 1,000

3.4 Influence of particle size on NF

The influence of particle size on NF in an MT at different Re and ϕ are presented in Figure 17A-D. With the reduction in NP size, the value of the HT coefficient is increased in an MT. The effect is, however, found insignificant at lower particle volume concentration, as presented in Figure 17A,C. At higher particle volume concentration, an abnormality is found for particle size 47 nm, as shown in Figure 17B,D. A significant decrease in h is registered for a 47-nm-sized particle as compared to the smaller size nanoparticles, probably attributed to a higher rate of settling for largest-sized nanoparticles.

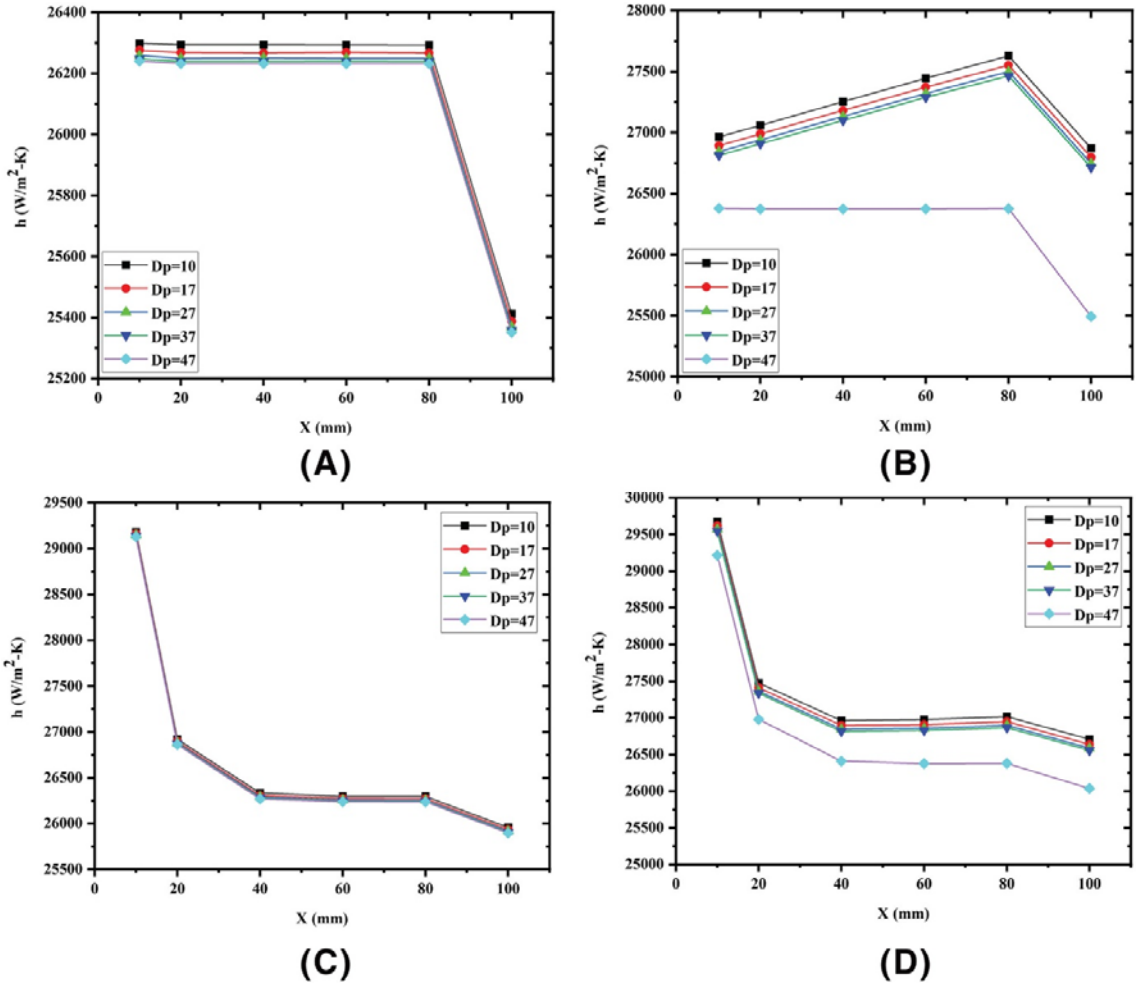

FIGURE 17. Effect of particle size on nanofluid in a microtube: (A) Re = 100, ϕ = 1%; (B) Re = 100, ϕ = 3%; (C) Re = 500, ϕ = 1%; and (D) Re = 500, ϕ = 3% .

The effect of particle size on NF in an MT at different Re and ϕ are presented in Figure 18A-D. For the wavy channel, the HT coefficient increases with the decrease in particle size as well. At lower ϕ, the influence of particle size is not significant as given in Figure 18A,C but a higher volume fraction effect is found significant in Figure 18B,D. Unlike MT, no abnormality is found for largest-sized (47 nm) particle flowing through the wavy channel as revealed from Figure 18B,D. This is probably due to the invigoration of nanoparticles while flowing through the channel due to its wavy nature, thereby reducing the settling rate to a great extent.

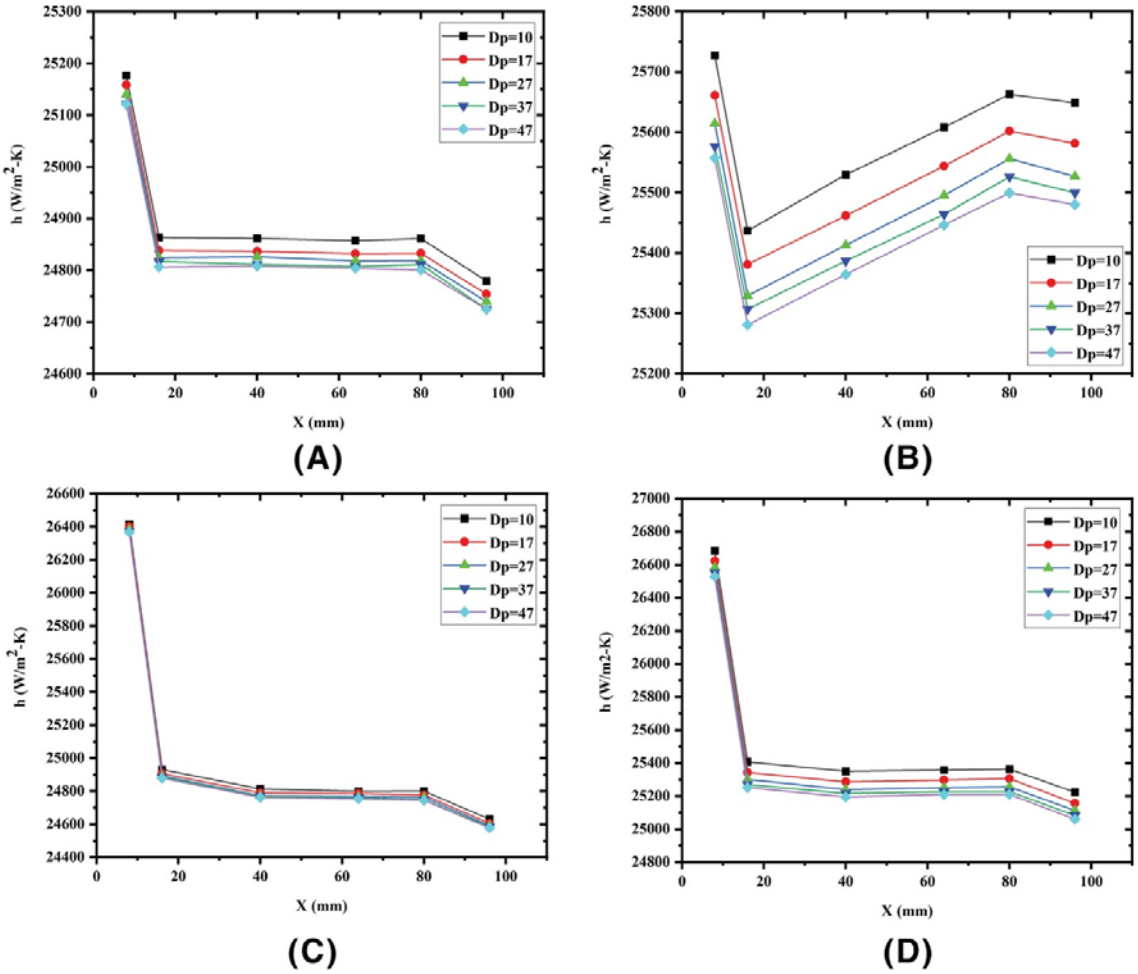

FIGURE 18. Effect of particle size on nanofluid in a wavy microchannel: (A) Re = 100, ϕ = 1%; (B) Re = 100, ϕ = 3%; (C) Re = 500, ϕ = 1%; and (D) Re = 500, ϕ = 3%

3.5 Friction factor analysis

Friction factor as a function of Reynolds number on NF and HNF in MT at volume fraction 3% is shown in Figure 19A. As expected, one can see from the figure that HNF is having a higher pressure drop than NF when it is flowing through MT. A similar result is depicted for WC at volume fraction 3% for HNF and NF in Figure 19B.

The influence of volume fraction on the friction factor in a MT at different Re is presented in Figure 19C. From the figure, one can see that there is no such effect of volume fraction (within a range of 1%-3%) is found on friction factor. The value of "f" becomes almost the same for all the tested volume fraction values. A similar trend was also found in the case of WC.

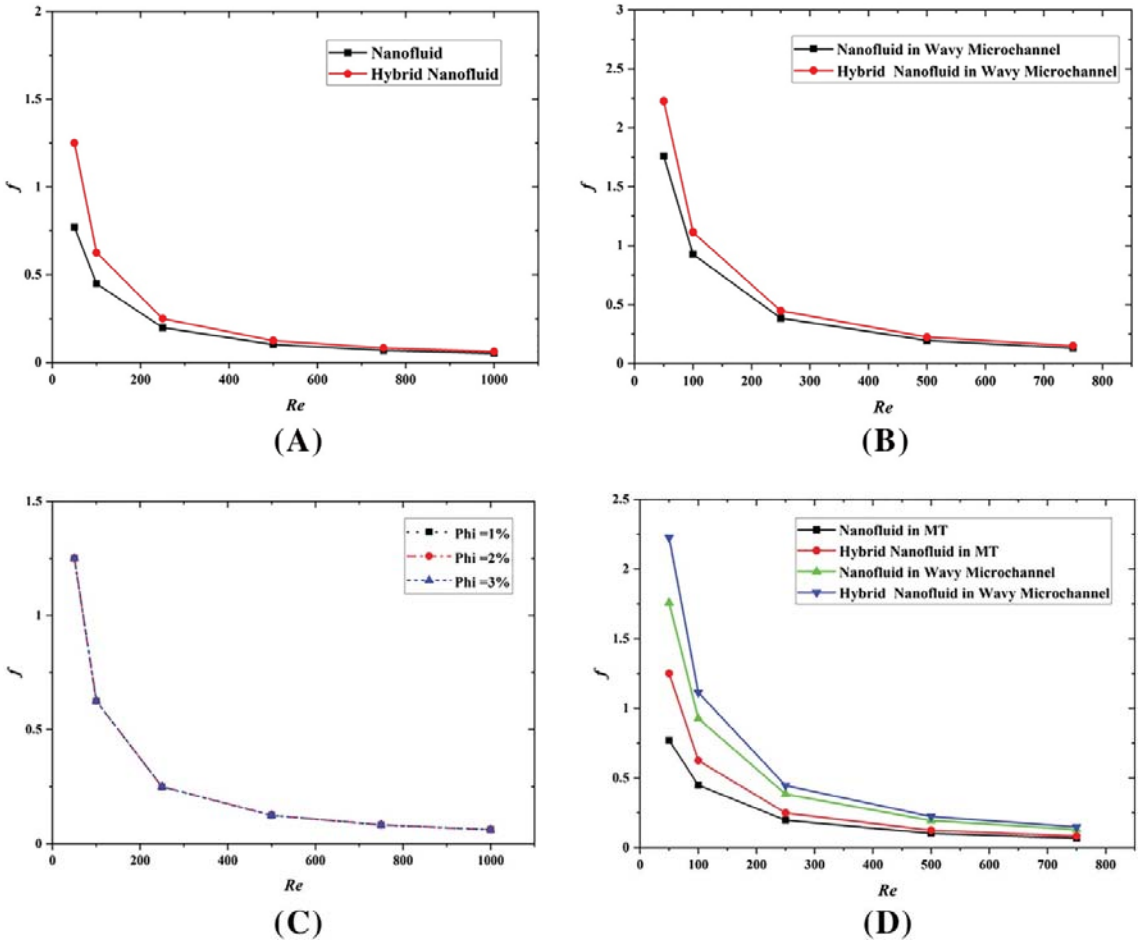

FIGURE 19. Friction factor as a function of Reynolds number: (A) comparison between hybrid nanofluid and nanofluid in microtube (MT) at ϕ = 3%, (A and B) comparison between hybrid nanofluid and nanofluid in wavy microchannel at ϕ = 3%, (C) variation of different phi for MT, and (D) comparison between wavy microchannel and MT at ϕ = 3%

Assessment of friction factor on NF and HNF in MT and WC at different Reynolds number and at constant volume fraction 3% is shown in Figure 4D. From the figure, one can understand and could summarize that the friction factor of HNF is higher than NFs. The HT augmentation generally depends on the value of TC of the fluid (base) and as well as NF. The TC of HNFs can augment HT by adding NPs of higher TC, which is also simultaneously increasing pressure drop.[98] Also, it is important to note that the value of the friction factor for WC is significantly higher than MT, this due to swirling effect and recirculation inside the WC. Almost all the complex structures of microchannels have better HT rate, which also increases the pressure drop due to eddies inside the channel.[98]

3.6 Comparison of all cases

Comparison of NF and HNF in MT and wavy channel are made to find the HT performance. Comparison of NF and HNF in MT and wavy channel at different Reynolds number are presented in Figure 20A-D. From the figures, we could conclude that the performance of HNF is better than NFs. Also, it is important to note that with constant heat flux, length, and area,

HT performance of MT is higher than the wavy channel while carrying NF as shown in Figure 20. At lower Reynolds number, HNF in MT is found most efficient for HT.

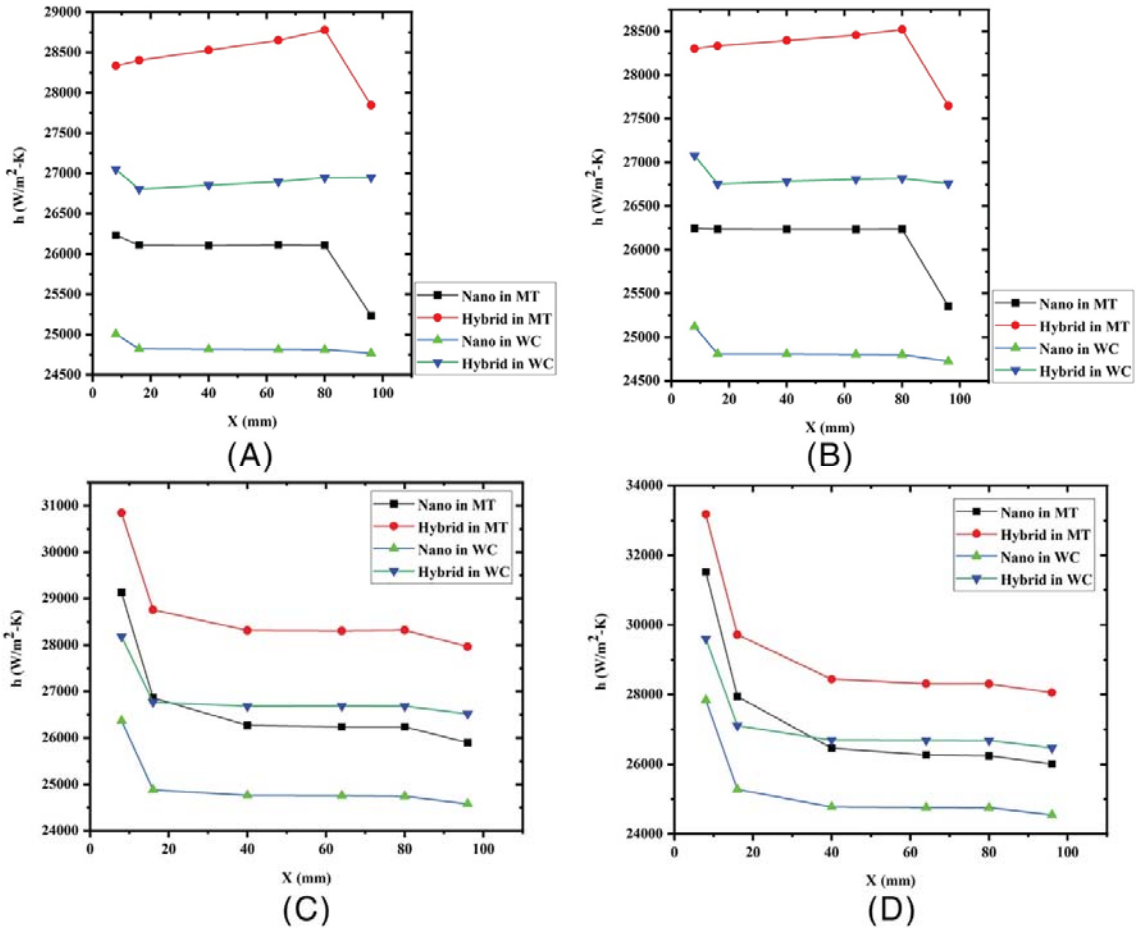

FIGURE 20. Comparison of nanofluid and hybrid nanofluid in microtube and wavy channel: (A) Re = 50, (B) Re = 100, (C) Re 500, and (D) Re = 1,000

4 CONCLUDING REMARKS

In the current work, a 2D numerical study is done to investigate the HT characteristics of Al_2O_3/water NF and Al_2O_3-Ag/water HNF flowing through a microchannel and WC at constant heat flux condition. Influence of Reynolds numbers, temperature, particle volume fraction, and nanoparticle size are considered to analyze the conjugate heat transfer phenomenon.

The conclusions from the current investigation are as follows:

- HNF has higher thermal energy transport coefficient as compared to NF and water, and water being the least HT coefficient among all three.
- Increase in Reynold number increases the local HT coefficient *h.*
- HT coefficient increases with an increase in particle ϕ.
- As the size of nanoparticle decreases, the local HT coefficient is increased for NF. The influence of NP size is prominent at a higher particle volume fraction.

- Al_2O_3/water NF is found almost independent of temperature while Al_2O_3-Ag/water HNF shows higher dependency on temperature.
- At higher Reynold numbers, heat transfer coefficient almost becomes independent of volume fraction for NF.
- At constant heat flux, MT shows better heat transfer characteristics than WC.

5 FUTURE SCOPE

The scientific community and manufacturing sector are moving toward the miniaturization, which leads to finding a better heat transfer fluid. NF shows the potential to fulfill that requirement. Hence, researchers start stepping to investigate the rheological and HT behavior of NFs as well as HNFs. Based on the present study, the following future works can be planned to understand the flow characteristics of NFs and HNFs:

- Multiphase modeling can be used in NFs and HNFs, which would provide better understanding of flow characteristics such as fluid-solid interaction and slip mechanism.
- Very few TC models are available for the properties of HNFs, and the models which are available did not consider all the governing parameters. Therefore, a vast research opportunity is available for the researchers to develop a dedicated TC model for HNFs by considering the various factors like clustering effect, Brownian motion, and size and shape of nanoparticles.

CONFLICTS OF INTEREST

This work does not have any conflicts of interest.

NOMENCLATURE

C_p	specific heat capacity [J/kg-K]
D	diameter of MT [m]
D_H	hydraulic diameter
h	heat transfer coefficient [W/m^2-K]
HNF	hybrid nanofluid
HT	heat transfer
k	thermal conductivity [W/m-K]
MC	microchannel
MT	microtube
NF	nanofluid
NP	nanoparticle
Pe	Peclet number (Re Pr)
Pr	Prandtl number ($\mu C_p/k$)
q''	heat flux [W/m^2]
R	madius of MT [m]
r, z	cylindrical coordinates [m]
Re	Reynolds number ($\rho U D_H/\mu$)
T	temperature [K]
TC	thermal conductivity
U	average velocity of nanofluid
u, v	velocity components [m/s]
WC	wavy microchannel

GREEK SYMBOLS

α thermal diffusivity, [m^2/s]
μ dynamic viscosity [Pa-s]
φ particle volume fraction, [%]

SUBSCRIPTS

bf base flluid
eff effective
f fluid
i inner
m mean
nf nanofluid
np nanoparticle
o outer
s solid
w wall

REFERENCES

1. Tuckerman DB, Pease RFW. High-performance heat sinking for VLSI. *IEEE Electron Device Lett*. 1981; 2(5): 126-129.
2. Choi SUS, Eastman JA. Enhancing thermal conductivity of fluids with nanoparticles. *Am Socf Mech Eng New York*. 1995; 66: 99-105.
3. Maxwell JC. A Treatise on Electricity and Magnetism. 2nd ed. 1 Oxford, U.K.: Clarendon Press; 1881.
4. Davis RH. The viscosity of suspensions of spherical particles. *Recueil des travauxchimiques des Payes-Bas*. 1942; 61: 863-887.
5. Hamilton RL, Crosser OK. Thermal conductivity of heterogeneous two component systems. *Ind Eng Chem Fund*. 1962; 1(3): 187-191.
6. Lu S, Lin H. Effective conductivity of composites containing aligned spheroidal inclusions of finite conductivity. *J Appl Phys*. 1996; 79(1): 6761-6769.
7. Yu W, Choi SUS. The role of interfacial layers in the enhanced thermal conductivity of nanofluids: a renovated Maxwell model. *J Nanopart Res*. 2003; 5(1/2): 167-171.
8. Jang SP, Choi SU. Role of Brownian motion in the enhanced thermal conductivity of nanofluids. *Appl Phys Lett*. 2004; 84(21): 4316-4318.
9. Chon CH, Kihm KD, Lee SP, Choi SUS. Empirical correlation finding the role of temperature and particle size for nanofluid (Al2O3) thermal conductivity enhancement. *Appl Phys*. 2005; 87(15):153107. https://doi.org/10.1063/1.2093936
10. Maiga SEB, Palm SJ, Nguyen CT, Roy G, Galanis N. Heat transfer enhancement by using nanofluids in forced convection flows. *Int J Heat Fluid Flow*. 2005; 26(4): 530-546.
11. Patel HE, Sundararajan T, Pradeep T, Dasgupta A, Dasgupta N, Das SK. A micro convection model for thermal conductivity of nanofluids. *Pramana J Phys*. 2005; 65(5): 863-869.
12. Jang P, Choi SUS. Effects of various parameters on nanofluid thermal conductivity. *J Heat Transfer*. 2007; 129(5): 617-623.
13. Murshed SMS, Leong KC, Yang C. A combined model for the effective thermal conductivity of nanofluids. *Appl Therm Eng*. 2009; 29(11–12): 2477-2483.
14. Corcione M. Empirical correlating equations for predicting the effective thermal conductivity and dynamic viscosity of nanofluids. *Energ Conver Manage*. 2011; 52(1): 789-793.

15. Jiang H, Xu Q, Huang C, Shi L. The role of interfacial nanolayer in the enhanced thermal conductivity of carbon nanotube-based nanofluids. *Appl Phys Mater Sci Process*. 2015; 118(1): 197-205.
16. Keblinski P, Phillpot SR, Choi SUS, Eastman JA. Mechanisms of heat flow in suspensions of nano-sized particles (nanofluids). *Int J Heat Mass Trans*. 2002; 45(4): 855-863.
17. Esfe MH, Wongwises S, Naderi A, et al. Thermal conductivity of Cu/TiO2–water/EG hybrid nanofluid: experimental data and modeling using artificial neural network and correlation. *Int Commun Heat Mass Trans*. 2015; 66: 100-104.
18. Toghraie D, Chaharsoghi VA, Afrand M. Measurement of thermal conductivity of ZnO–TiO2/EG hybrid nanofluid. *J Ther Anal Calorimetr*. 2016; 125(1): 527-535.
19. Parsian A, Akbari M. New experimental correlation for the thermal conductivity of ethylene glycol containing Al2O3–Cu hybrid nanoparticles. *J Ther Anal Calorimetr*. 2018; 131(2): 1605-1613.
20. Einstein A. A new determination of the molecular dimensions. *Ann Phys Rehabil Med*. 1906; 324(2): 289-306.
21. Brinkman HC. The viscosity of concentrated suspensions and solutions. *J Chem Phys*. 1952; 20(4): 571-581.
22. Batchelor G. The effect of Brownian motion on the bulk stress in a suspension of spherical particles. *J Fluid Mech*. 1977; 83(1): 97-117.
23. Pak BC, Cho YI. Hydrodynamic and heat transfer study of dispersed fluids with submicron metallic oxide particles. *Exper Ther Fluid Sci J*. 1998; 11: 151-170.
24. Nguyen C, Desgranges F, Roy G, Galanis N, Mare T, Boucher S. Temperature and particle size dependent viscosity data for water-based nanofluids–hysteresis phenomenon. *Int J Heat Fluid Flow*. 2007; 28(6): 1492-1506.
25. Abu-Nada E. Effects of variable viscosity and thermal conductivity of Al2O3–water nanofluid on heat transfer enhancement in natural convection. *Int J Heat Fluid Flow*. 2009; 30(4): 679-690.
26. Turcu R, Darabont A, Nan A, Aldea N, Macovei D, Bica D. New polypyrrole multiwall carbon nanotubes hybrid materials. *J Optoelectron Adva Mater*. 2006; 8: 643-647.
27. Bhattacharya P, Samanta AN, Chakraborty S. Numerical study of conjugate heat transfer in rectangular microchannel heat sink with Al2O3/H2O nanofluid. *Heat Mass Trans*. 2009; 45(10): 1323-1333.
28. Singh PK, Harikrishna PV, Sundararajan T, Das SK. Experimental and numerical investigation into the heat transfer study of nanofluids in microchannel. *J Heat Trans ASME*. 2011; 133(12): 121701. https://doi.org/10.1115/1.4004430
29. Lelea D, Nisulescu D. The micro-tube heat transfer and fluid flow of water based Al_2O_3 nanofluid with viscous dissipation. *Int Commun Heat Mass Trans*. 2011; 38(6): 704-710.
30. Nimmagadda R, Venkatasubbaiah K. Conjugate heat transfer analysis of micro-channel using novel hybrid nanofluids (Al_2O_3+Ag/water). *Eur J Mech B/Fluids*. 2015; 52: 19-27.
31. Selvakumar P, Suresh S. Use of Al_2O_3–Cu/water hybrid nanofluid in an electronic heat sink. IEEE Transactions on Components. *Packag Manuf Technol*. 2012; 2(10): 1600-1607.
32. Yang YT, Wang YH, Tseng PK. Numerical optimization of heat transfer enhancement in a wavy channel using nanofluids. *Int Commun Heat Mass Trans*. 2014; 51: 9-17.

33. Sakanov A, Keian CC, Zhao J. Performance improvements of microchannel heat sink using wavy channel and nanofluids. *Int J Heat Mass Trans*. 2015; 89: 59-74.
34. Bhattacharyya S, Chattopadhyay H, Benim AC. Computational investigation of heat transfer enhancement by alternating inclined ribs in tubular heat exchanger. *Prog Computat Fluid Dyn Intl J*. 2017; 17(6): 390-396.
35. Bhattacharyya S, Chattopadhyay H, Guin A, Benim AC. Investigation of inclined turbulators for heat transfer enhancement in a solar air heater. *Heat Transfer Engineering*. 2019; 40(17–18): 1451-1460.
36. Bhattacharyya S, Chattopadhyay H, Saha SK. Numerical Study on heat transfer enhancement of laminar flow through a circular tube with artificial rib roughness. *J Refrig, Air Condition, Heat Ventilation*. 2014; 1(3): 14-19.
37. Bhattacharyya S, Chattopadhyay H, Benim AC. Heat transfer enhancement of laminar flow of ethylene glycol through a square channel fitted with angular cut wavy strip. *Proc Eng*. 2016; 157: 19-28.
38. Bhattacharyya S, Chattopadhyay H, Biswas R, Ewim DRE, Huan Z. Influence of inlet turbulence intensity on transport phenomenon of modified diamond cylinder: a numerical study. *Arab J Sci Eng*. 2020; 45(2): 1051-1058.
39. Chamkha AJ, Rashad AM, Alsabery AI, Abdelrahman ZMA, Nabwey HA. Impact of partial slip on magneto-ferrofluids mixed convection flow in enclosure. *J Therm Sci Eng Appl*. 2020, pp. 051002–051001; 12(5):051002. https://doi.org/10.1115/1.4046060
40. Tayebi T, Chamkha AJ. Enclosure in the presence of a wavy circular conductive cylinder. *Journal of Thermal Science and Engineering Applications*. 2020; 12(3):031009.
41. Mehryan SAM, Ghalambaz M, Chamkha AJ, Izadi M. Numerical study on natural convection of Ag–MgO hybrid/water nanofluid inside a porous enclosure: a local thermal nonequilibrium model. *Powder Technol*. 2020; 367: 443-455.
42. Krishna MV, Ahmed NA, Chamkha NAJ. Heat and mass transfer on magnetohydrodynamic convective flow of second grade fluid through a vertical porous channel with non-uniform wall temperature. *Adv Sci Eng Med*. 2020; 12(3): 376-387.
43. Mansoury D, Doshmanziari FI, Kiani A, Chamkha AJ, Sharifpur M. Heat transfer and flow characteristics of AL_2O_3/water nanofluid in various heat exchangers: experiments on counter flow. *Heat Trans Eng*. 2020; 41(3): 220-234.
44. Sadeghi HM, Babayan M, Chamkha A. Investigation of using multi-layer PCMs in the tubular heat exchanger with periodic heat transfer boundary condition. *Int J Heat Mass Trans*. 2020; 147: 118970. https://doi.org/10.1016/j.ijheatmasstransfer.2019.118970
45. Dogonchi AS, Nayak MK, Karimi N, Chamkha AJ, Ganji DD. Numerical simulation of hydrothermal features of Cu–H_2O nanofuid natural convection within a porous annulus considering diverse configurations of heater. *J Ther Anal Calorimetr*. Online Published. 2020. https://doi.org/10.1007/s10973-020-09419-y
46. Ghalambaz M, Doostani A, Izadpanahi E, Chamkha AJ. Conjugate natural convection flow of Ag–MgO/water hybrid nanofluid in a square cavity. *J Ther Anal Calorimetr*. 2020; 139(3): 2321-2336.

47. Ishak MS, Alsabery AI, Chamkha A, Hashim I. Effect of finite wall thickness on entropy generation and natural convection in a nanofluid-filled partially heated square cavity. *Int J Numer Method Heat Fluid Flow*. 2020; 30(3): 1518-1546.
48. Rejvani M, Saedodin S, Vahedi SM, Wongwises S, Chamkha AJ. Experimental investigation of hybrid nano-lubricant for rheological and thermal engineering applications. *J Ther Anal Calorimetr*. 2019; 138: 1823-1839.
49. Alsabery AI, Mohebbi R, Chamkha AJ, Hashim I. Impacts of magnetic field and non-homogeneous nanofluid model on convective heat transfer and entropy generation in a cavity with heated trapezoidal body. *J Ther Anal Calorimetr*. 2019; 138(2): 1371-1394.
50. Mehryan SAM, Izadi M, Namazian Z, Chamkha AJ. Natural convection of multi-walled carbon nanotube–Fe3O4/water magnetic hybrid nanofluid flowing in porous medium considering the impacts of magnetic field-dependent viscosity. *J Ther Anal Calorimetr*. 2019; 138(2): 1541-1555.
51. Hoseinzadeh S, Heyns PS, Chamkha AJ, Shirkhani A. Thermal analysis of porous fins enclosure with the comparison of analytical and numerical methods. *J Ther Anal Calorimetr*. 2019; 138(1): 727-735.
52. Taamneh Y, Kabeel AE, Prakash N, Sathyamurthy R, Chamkha AJ. Thermal and hydraulic characteristics of a triangular duct using an Al_2O_3 nanofluid in a turbulent flow regime. *Heat Transfer—Asian Res*. 2019; 48(6): 2639-2654.
53. Raza J, Mebarek-Oudina F, Chamkha AJ. Magnetohydrodynamic flow of molybdenum disulfide nanofluid in a channel with shape effects. *Multidiscip Model Maternd Struct*. 2019; 15(4): 737-757.
54. Giwa SO, Sharifpur M, Meyer JP. Effects of uniform magnetic induction on heat transfer performance of aqueous hybrid ferrofluid in a rectangular cavity. *Appl Therm Eng*. 2020; 170: 115004. https://doi.org/10.1016/j.applthermaleng.2020.115004
55. Giwa SO, Sharifpur M, Meyer JP. Experimental study of thermo-convection performance of hybrid nanofluids of Al_2O_3-MWCNT/water in a differentially heated square cavity. *Int J Heat Mass Trans*. 2020; 148: 119072. https://doi.org/10.1016/j.ijheatmasstransfer.2019.119072
56. Osman S, Sharifpur M, Meyer JP. Experimental investigation of convection heat transfer in the transition flow regime of aluminium oxide-water nanofluids in a rectangular channel. *Int J Heat Mass Trans*. 2019; 133: 895-902.
57. Mahdavi M, Garbadeen I, Sharifpur M, Ahmadi MH, Meyer JP. Study of particle migration and deposition in mixed convective pipe flow of nanofluids at different inclination angles. *J Ther Anal Calorimetr*. 2019; 135(2): 1563-1575.
58. Sharifpur M, Solomon AB, Ottermann TL, Meyer JP. Optimum concentration of nanofluids for heat transfer enhancement under cavity flow natural convection with TiO_2–water. *Int Commun Heat Mass Trans*. 2018; 98: 297-303.
59. Sharifpur M, Tshimanga N, Meyer JP, Manca O. Experimental investigation and model development for thermal conductivity of α-Al_2O_3-glycerol nanofluids. *Int Commun Heat Mass Trans*. 2017; 85: 12-22.
60. Jilte R, Ahmadi MH, Kumar R, Kalamkar V, Mosavi A. Cooling performance of a novel circulatory flow concentric multi-channel heat sink with nanofluids. *Nanomaterials*. 2020; 10(4): 647. https://doi.org/10.3390/nano10040647

61. Sharma JP, Sharma A, Jilte RD, Kumar R, Ahmadi MH. A study on thermohydraulic characteristics of fluid flow through microchannels. *J Ther Anal Calorimetr*. 2020; 140(1): 1-3.
62. Beigzadeh M, Pourfayaz F, Ahmadi MH. Modeling and improvement of solid oxide fuel cell-single effect absorption chiller hybrid system by using nanofluids as heat transporters. *Appl Therm Eng*. 2020; 166: 114707.
63. Aghayari R, Maddah H, Pourkiaei SM, Ahmadi MH, Chen L, Ghazvini M. Theoretical and experimental studies of heat transfer in a double-pipe heat exchanger equipped with twisted tape and nanofluid. *Eur Phys J Plus*. 2020; 135(2): 1-26.
64. Abadi E, Mohammad A, Sadi M, et al. A numerical and experimental study on the energy efficiency of a regenerative heat and mass exchanger utilizing the counter-flow Maisotsenko cycle. *Eng Appl Computat Fluid Mech*. 2020; 14(1): 1-12.
65. Ahmadi MH, Ghazvini M, Maddah H, et al. Prediction of the pressure drop for CuO/(ethylene glycol-water) nanofluid flows in the car radiator by means of artificial neural networks analysis integrated with genetic algorithm. *Phys A Stat Mech Appl*. 2020; 546: 124008.
66. Heydar M, Ghazvini M, Ahmadi MH. Predicting the efficiency of CuO/water nanofluid in heat pipe heat exchanger using neural network. *Int Commun Heat Mass Trans*. 2019; 104: 33-40.
67. Ghahremannezhad A, Xu H, Nazari MA, Ahmadi MH, Vafai K. Effect of porous substrates on thermohydraulic performance enhancement of double layer microchannel heat sinks. *Int J Heat Mass Trans*. 2019; 131: 52-63.
68. Gan T, Ming T, Fang W, et al. Heat transfer enhancement of a microchannel heat sink with the combination of impinging jets, dimples, and side outlets. *J Ther Anal Calorimetr*. 2020; 141: 45-56.
69. Dogonchi AS, Sheremet MA, Ganji DD, Pop I. Free convection of copper–water nanofluid in a porous gap between hot rectangular cylinder and cold circular cylinder under the effect of inclined magnetic field. *J Ther Anal Calorimetr*. 2019; 135(2): 1171-1184. https://doi.org/10.1007/s10973-018-7396-3
70. Esfe MH, Firouzi M, Rostamian H, Afrand M. Prediction and optimization of thermophysical properties of stabilized Al2O3/antifreeze nanofluids using response surface methodology. *J Mol Liq*. 2018; 261: 14-20. https://doi.org/10.1016/j.molliq.2018.03.063
71. Ghahremani E. Transient natural convection in an enclosure with variable thermal expansion coefficient and nanofluid properties. *J Appl Comput Mech*. 2018; 4(3): 133-139. https://doi.org/10.22055/JACM.2017.22206.1128
72. Izadi M, Hoghoughi G, Mohebbi R, Sheremet M. Nanoparticle migration and natural convection heat transfer of Cu-water nanofluid inside a porous undulant-wall enclosure using LTNE and two-phase model. *J Mol Liq*. 2018; 261: 357-372. https://doi.org/10.1016/j.molliq.2018.04.063
73. Mehryan SAM, Izadi M, Chamkha AJ, Sheremet MA. Natural convection and entropy generation of a ferrofluid in a square enclosure under the effect of a horizontal periodic magnetic field. *J Mol Liq*. 2018; 263: 510-525. https://doi.org/10.1016/j.molliq.2018.04.119
74. Alsabery AI, Mohebbi R, Chamkha AJ, Hashim I. Effect of local thermal non-equilibrium model on natural convection in a nanofluid-filled wavy-walled porous

cavity containing inner solid cylinder. *Chem Eng Sci*. 2019; 201: 247-263. https://doi.org/10.1016/j.ces.2019.03.006
75. Dogonchi AS, Armaghani T, Chamkha AJ, Ganji DD. Natural convection analysis in a cavity with an inclined elliptical heater subject to shape factor of nanoparticles and magnetic field. *Arab J Sci Eng*. 2019; 44(9): 7919-7931. https://doi.org/10.1007/s13369-019-03956-x
76. Hoseinzadeh S, Moafi A, Shirkhani A, Chamkha AJ. Numerical validation heat transfer of rectangular cross-section porous fins. *J Thermophys Heat Trans*. 2019; 33(3): 698-704. https://doi.org/10.2514/1.T5583
77. Kumar B, Seth GS, Nandkeolyar R, Chamkha AJ. Outlining the impact of induced magnetic field and thermal radiation on magneto-convection flow of dissipative fluid. *Int J Therm Sci*. 2019; 146:106101. https://doi.org/10.1016/j.ijthermalsci.2019.106101
78. Shashikumar NS, Gireesha BJ, Mahanthesh B, Prasannakumara BC, Chamkha AJ. Entropy generation analysis of magneto-nanoliquids embedded with aluminium and titanium alloy nanoparticles in microchannel with partial slips and convective conditions. *Int J Numer Method Heat Fluid Flow*. 2019; 29(10): 3638-3658. https://doi.org/10.1108/HFF-06-2018-0301
79. Sobamowo MG. Free convection flow and heat transfer of nanofluids of different shapes of nano-sized particles over a vertical plate at low and high Prandtl numbers. *J Appl Comput Mech*. 2019; 5(1): 13-39. https://doi.org/10.22055/JACM.2018.24529.1196
80. Tayebi T, Chamkha AJ. Entropy generation analysis during MHD natural convection flow of hybrid nanofluid in a square cavity containing a corrugated conducting block. *Int J Numer Method Heat Fluid Flow*. 2020; 30(3): 1115-1136. https://doi.org/10.1108/HFF-04-2019-0350
81. Ghalambaz M, Chamkha AJ, Wen D. Natural convective flow and heat transfer of nano-encapsulated phase change materials (NEPCMs) in a cavity. *Int J Heat Mass Trans*. 2019a; 138: 738-749. https://doi.org/10.1016/j.ijheatmasstransfer.2019.04.037
82. Ghalambaz M, Mehryan SAM, Izadpanahi E, Chamkha AJ, Wen D. MHD natural convection of Cu–Al2O3 water hybrid nanofluids in a cavity equally divided into two parts by a vertical flexible partition membrane. *J Ther Anal Calorimetr*. 2019b; 138(2): 1723-1743. https://doi.org/10.1007/s10973-019-08258-w
83. Alsabery AI, Armaghani T, Chamkha AJ, Hashim I. Two-phase nanofluid model and magnetic field effects on mixed convection in a lid-driven cavity, containing heated triangular wall. *Alex Eng J*. 2020; 59(1): 129-148. https://doi.org/10.1016/j.aej.2019.12.017
84. Dogonchi AS, Tayebi T, Chamkha AJ, Ganji DD. Natural convection analysis in a square enclosure with a wavy circular heater under magnetic field and nanoparticles. *J Ther Anal Calorimetr*. 2020; 139(1): 661-671. https://doi.org/10.1007/s10973-019-08408-
85. Hajjar A, Mehryan SAM, Ghalambaz M. Time periodic natural convection heat transfer in a nano-encapsulated phase-change suspension. *Int J Mech Sci*. 2020; 166: 105243. https://doi.org/10.1016/j.ijmecsci.2019.105243
86. Hashemi-Tilehnoee M, Dogonchi AS, Seyyedi SM, Chamkha AJ, Ganji DD. Magnetohydrodynamic natural convection and entropy generation analyses inside a

nanofluid-filled incinerator-shaped porous cavity with wavy heater block. *J Ther Anal Calorimetr*. 2020. https://doi.org/10.1007/s10973-019-09220-6
87. Chamkha AJ, Sazegar S, Jamesahar E, Ghalambaz M. Thermal non-equilibrium heat transfer modeling of hybrid nanofluids in a structure composed of the layers of solid and porous media and free nanofluids. *Energies*. 2019; 12(541): 1-27. https://doi.org/10.3390/en12030541
88. Mehryan SAM, Izadpanahi E, Ghalambaz M, Chamkha AJ. Mixed convection flow caused by an oscillating cylinder in a square cavity filled with Cu–Al2O3/water hybrid nanofluid. *J Ther Anal Calorimetr*. 2019; 137(3): 965-982. https://doi.org/10.1007/s10973-019-08012-2
89. Aparna Z, Michael M, Pabi SK, Ghosh S. Thermal conductivity of aqueous Al2O3/Ag hybrid nanofluid at different temperatures and volume concentrations: an experimental investigation and development of new correlation function. *Powder Technol*. 2019; 343: 714-722. https://doi.org/10.1016/j.powtec.2018.11.096
90. Jastrzebska AM, Kunicki AR, Olszyna AR, Karwowska E. Al2O3–Ag nanopowders: new method of synthesis, characterisation and biocidal activity. *Adv Appl Ceram*. 2011; 110(2): 108-113. https://doi.org/10.1179/1743676110Y.0000000014
91. Perry R, Green D. Perry's Chemical Engineers' Handbook. New York, NY: McGraw-Hill; 1999.
92. Kaska SA, Khalefa RA, Hussein AM. Hybrid nanofluid to enhance heat transfer under turbulent flow in a flat tube. *Case Stud Ther Eng*. 2019; 13: 100398.
93. Bhattacharyya S, Vishwakarma DK, Roy S, Biswas R, Ardekani MM. Applications of heat transfer enhancement techniques: a state-of-the-art review. *Inverse Heat Conduction and Heat Exchangers*, Online Published. 2020. https://doi.org/10.5772/intechopen.92873
94. Everts M, Bhattacharyya S, Bashir AI, Meyer JP. Heat transfer characteristics of assisting and opposing laminar flow through a vertical circular tube at low Reynolds numbers. *Appl Therm Eng*. 2020; 179:115696. https://doi.org/10.1016/j.applthermaleng.2020.115696
95. Bhattacharyya S, Souayeh B, Banerjee A, Sarkar R, Rahimi-Gorji M, Nguyen HM. Numerical analysis of micro-pin-fin heat sink cooling in the mainboard chip of a CPU. *Eur Phys J Plus*. 2020; 135(6): 432. https://doi.org/10.1140/epjp/s13360-020-00359-y
96. Alam MW, Bhattacharyya S, Souayeh B, et al. CPU heat sink cooling by triangular shape micro-pin-fin: numerical study. *Int Commun Heat Mass Trans*. 2020; 112:104455. https://doi.org/10.1016/j.icheatmasstransfer.2019.104455
97. Bhattacharyya S, Das S, Sarkar A, Guin A, Mullick A. Numerical simulation of flow and heat transfer around hexagonal cylinder. *Int J Heat Technol*. 2017; 35(2): 360-363. https://doi.org/10.18280/ijht.350218
98. Kumar H, Sokhal GS. Effect of geometries and nanofluids on heat transfer and pressure drop in microchannels: a review. *Mater Today Proc*, Online Published. 2020. https://doi.org/10.1016/j.matpr.2020.05.288